Prepared for submission to JHEP

Holographic Dual to Conical Defects: I. Moving Massive Particle

D.S. Ageev[a] **I.Ya. Aref'eva**[a] **M.D. Tikhanovskaya**[b]

[a] *Steklov Mathematical Institute, Russian Academy of Sciences, Gubkin str. 8, 119991 Moscow, Russia*

[b] *National Research Nuclear University "MEPhI" (Moscow Engineering Physics Institute), 115409 Moscow, Russia*

E-mail: ageev@mi.ras.ru, arefeva@mi.ras.ru, tikhanovskaya@mi.ras.ru

Abstract: We study correlation functions of scalar operators on the boundary of the AdS_3 space deformed by moving massive particles in the context of the AdS/CFT duality. To calculate two-point correlation functions we use the geodesic approximation and the renormalized image method. We compare results of the renormalized image method with direct calculations using tracing of winding geodesics around the cone singularities, and show on examples that they are equivalent. We demonstrate that in the geodesic approximation the correlators exhibit a zone structure. This structure substantially depends on the mass and velocity of the particle.

Keywords: AdS/CFT correspondence, holography, conical defects, thermalization

arXiv:1512.03362v2 [hep-th] 5 May 2016

Contents

1 Introduction **2**

2 Setup **3**
- 2.1 AdS_3 space as a group manifold 3
- 2.2 Point particles in AdS_3 4
  - 2.2.1 Static particle in AdS_3 4
  - 2.2.2 Moving massive particle in the AdS_3 5
- 2.3 Correlation functions on the boundary and geodesics in the AdS_3. 8
  - 2.3.1 Spacelike separated points 9
  - 2.3.2 Timelike separated points 11
  - 2.3.3 Reflection symmetry 13
  - 2.3.4 Remarks about the Wightman, causal and retarded correlators 13

3 Image method and winding geodesics **15**
- 3.1 Image method on the living space 15
- 3.2 Static defect. 18
  - 3.2.1 Equal-time points. 18
  - 3.2.2 Proof of periodicity 20
  - 3.2.3 Spacelike separated points 21
  - 3.2.4 Universal formula and isometry invariance 22
- 3.3 Moving particle. 22
  - 3.3.1 Light moving massive particle 23
  - 3.3.2 Heavy moving massive particle 24
- 3.4 Renormalization 26
  - 3.4.1 Spacelike geodesics 26
  - 3.4.2 Quasigeodesics 27

4 Zone structure of correlators **29**
- 4.1 Light particle 29
- 4.2 Heavy particle 30

5 Conclusion **34**

1 Introduction

The AdS/CFT, or more generally the gauge/gravity duality [1–3] is a powerful tool in the study of quantum systems in the strong coupling limit. Due to its flexibility there is a wide range of applications in heavy-ion collision [4–6], condensed matter theory [7–9], thermalization of strongly coupling theories [10–14], entanglement entropy [15–17] and quantum quenches [18, 19].

Two dimensional conformal field theory is the holographic dual of AdS_3 gravity. Three dimensional gravity is topological and there are no propagating gravitons in this theory. Deformations of the three-dimensional gravity by point particles are only global [20, 21]. This means, that locally the deformed space is still the AdS_3, but globally there are wedges to cut out and glue their faces. In another words, point particles induce conical singularities. Scattering of point particles in the space with conical singularities was studied in [22]. Classical and quantum scalar field theories on a cone have been considered in several papers starting from [23] and scalar fields in the flat space with defects have been studied in [24]. The cosmic strings in the flat M_4 and AdS_4 provide four-dimensional generalization [25–27], while the cosmic membranes provide higher dimensional generalization of conical defect in the context of the TeV-gravity [28].

In is natural to ask a question about holographic dual to AdS_3 with point particles [29]. Correlators in the theory dual to AdS_3 with a static particle have been considered within the geodesic approximation [29, 30] and appearance of new excitations in the boundary theory has been noticed. Then, the AdS/CFT correspondence for the multi-boundary AdS_3 orbifold has been studied [31]. A new quantity, called entwinement, in the dual CFT has been introduced in [32], and it has been shown that it is related with the conical defect geometry. Correlators in the theory dual to the Gott time machine in the AdS_3 have been investigated [33]. A holographic dual model for defect conformal field theories has been considered in [34].

In this paper we continue to study boundary theories dual to AdS_3 deformed by massive moving point particles. To describe these deformations it is convenient to consider AdS_3 as an $SL(2,R)$ group manifold [35]. AdS_3 with a particle is a space that remains after cutting out a special subset, called wedge, from AdS_3 spacetime, and then identifying the boundaries of this wedge in a special way [21, 36]. The geodesics in this spacetime locally are the same as in the nondeformed AdS_3 and this drastically simplifies the problem of constructing the boundary correlators in the geodesic approximation. In the geodesic approximation one has to find all geodesics connecting two given points on the boundary. For one static particle one can find all geodesics connecting two spacelike separated points explicitly in the Deser-Jackiw coordinates [32]. But the generalization of these coordinates to multi-particle cases is not explicit [37] which makes the problem of analytical description of all geodesics rather complicated.

We study this problem using the cutting and gluing method that has been used previously in [29, 30, 32, 33]. As in [33], in this paper we have to use numerical simulations to take into account all geodesics connecting two given points on the boundary in the present of moving defects.

The paper is organized as follows. In Section 2, we remind the group structure of the AdS_3 and set the notations. In Section 3, the renormalized image method is described. The relation of winding geodesics and imaged geodesics is clarified on several examples. In Section 4, the zone structure of correlators on the boundary of the AdS_3 deformed by moving particle is presented and discussed.

2 Setup

2.1 AdS_3 space as a group manifold

In this section we set the notations and the parametrization we use in this paper. The AdS_3 is a hyperboloid, which in embedding coordinates x_0, x_1, x_2 and x_3 can be written as:

$$-x_0^2 - x_3^2 + x_1^2 + x_2^2 = -1. \tag{2.1}$$

We also use the barrel coordinates (t, χ, ϕ):

$$\begin{aligned} x_3 &= \cosh\chi \cos t, \\ x_0 &= \cosh\chi \sin t, \\ x_1 &= \sinh\chi \cos\phi, \\ x_2 &= \sinh\chi \sin\phi, \end{aligned} \tag{2.2}$$

where t is the time coordinate, χ is the radial coordinate and ϕ is the angular coordinate with period 2π. The AdS_3 conformal boundary corresponds to $\chi \to \infty$. In these coordinates the metric can be written out as:

$$ds^2 = -\cosh^2\chi dt^2 + d\chi^2 + \sinh^2\chi d\phi^2.$$

Instead of χ and ϕ also we will use Poincare disc coordinates related with χ as $r = \tanh\chi/2$ and in these coordinates the metric has the form:

$$ds^2 = -\left(\frac{1+r^2}{1-r^2}\right)^2 dt^2 + \left(\frac{2}{1-r^2}\right)^2 (dr^2 + r^2 d\phi^2).$$

The AdS_3 also admits the representation as $SL(2,R)$ group of real 2x2 matrices:

$$\mathbf{x} = x_3\mathbf{1} + \sum_{\mu=0,1,2} \gamma_\mu x^\mu = \cosh\chi\, \mathbf{\Omega}(t) + \sinh\chi\, \mathbf{\Gamma}(\phi) = \begin{pmatrix} x_3 + x_2 & x_0 + x_1 \\ x_1 - x_0 & x_3 - x_2 \end{pmatrix}, \tag{2.3}$$

where

$$\mathbf{1} = \begin{pmatrix} 1 & 0 \\ 0 & 1 \end{pmatrix}; \quad \gamma_0 = \begin{pmatrix} 0 & 1 \\ -1 & 0 \end{pmatrix}; \quad \gamma_1 = \begin{pmatrix} 0 & 1 \\ 1 & 0 \end{pmatrix}; \quad \gamma_2 = \begin{pmatrix} 1 & 0 \\ 0 & -1 \end{pmatrix}, \tag{2.4}$$

and

$$\mathbf{\Omega}(t) = \cos t\mathbf{1} + \sin t\gamma_0; \quad \mathbf{\Gamma}(\phi) = \cos\phi\gamma_1 + \sin\phi\gamma_2. \tag{2.5}$$

The condition $\det \mathbf{x} = 1$ is equivalent to (2.1)

2.2 Point particles in AdS_3

It is known, that the gravity in spacetime dimension 3 is almost trivial, in the sense of absence of propagating degrees of freedom. In works [20, 21] it was shown, that point particle does not change the metric locally, producing conical defect singularity. In this section we remind the structure of the AdS_3 deformed by point particles.

2.2.1 Static particle in AdS_3

Let us recall the Deser-Jackiw solution [20]. Consider the Einstein equation in the 3-dimensional spacetime with the cosmological constant which equals to -1 :

$$G^{\mu\nu} - g^{\mu\nu} = 8\pi G T^{\mu\nu}. \tag{2.6}$$

The ansatz for the metric ds^2_{DJ} supported by the time independent point-like source is:

$$\begin{aligned} ds^2_{DJ} &= -N^2(R)dt^2 + \Phi(R)(dR^2 + R^2 d\tilde{\phi}^2), \\ T^{00} &= \frac{m}{\sqrt{-g}} N(R)\delta(R), \end{aligned}$$

where functions $\Phi(R)$ and $N(R)$ are:

$$\Phi(R) = \frac{4A^2}{\Lambda R^2 \left((R/R_0)^A + (R/R_0)^{-A}\right)^2}, \qquad N(R) = \frac{\left((R/R_0)^A - (R/R_0)^{-A}\right)}{\left((R/R_0)^A + (R/R_0)^{-A}\right)}$$

Parameter A connects with the mass of the particle as $A = 1 - 4Gm$. After the change of variables:

$$\sinh\chi = \frac{1}{2}\left(\left(\frac{R}{R_0}\right)^A + \left(\frac{R}{R_0}\right)^{-A}\right), \quad \phi = A\tilde{\phi},$$

we get the AdS_3 metric in the barrel coordinates with a different angular coordinate range of values,

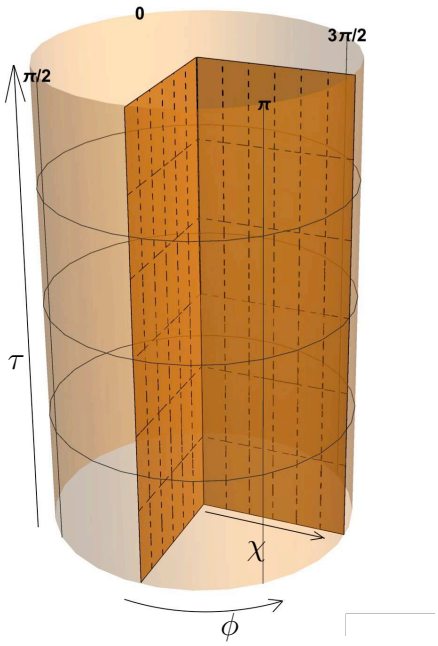

Figure 1. The AdS_3 deformed by the static particle. Two constant angle surfaces incident from the origin of the AdS are the faces of the wedge to cut out and identify.

$$ds^2 = -\cosh^2\chi dt^2 + d\chi^2 + \sinh^2\chi d\phi^2, \quad \phi \in (0, 2\pi A)\,.$$

Let us now consider the static particle case from the group language. Resting in the center of the AdS_3 static particle cuts out the wedge that can be described by two faces that are some constant angle surfaces (see Fig.1). These two faces are identified in the constant t sections. In matrix notation the first face of the wedge is:

$$\mathbf{x}_{1-st\,face} = \cosh\chi\,\mathbf{\Omega}(t) + \sinh\chi\,\mathbf{\Gamma}(-\alpha/2). \tag{2.7}$$

The face is parameterized by two values: α and t, α is proportional to the mass of the particle and t is time coordinate. The second face of the wedge can be obtained by rotation of the first face by the angle α. Writing out rotation:

$$\mathbf{x}_{rot} = u_{rot}^{-1}\,\mathbf{x}\,u_{rot}, \quad u_{rot} = \mathbf{\Omega}(-\alpha/2),$$

we get the second face:

$$\mathbf{x}_{2-nd\,face} = \mathbf{\Omega}(\alpha/2)\,\cdot\,\mathbf{x}_{1-st\,face}\,\cdot\,\mathbf{\Omega}(-\alpha/2), \tag{2.8}$$

where $\mathbf{\Omega}(\alpha/2)$ is given by (2.5).

2.2.2 Moving massive particle in the AdS_3

To consider a massive moving particle and get it's group language description one can consider a static particle and boost it. The massive particle moves along the periodic worldline oscillating in the bulk of the AdS_3. The constant angle faces of

the wedge to be identified become some surfaces that one can get by boosting the wedge of the static particle. These faces are glued as in the static case along the constant time slices and symmetrically with respect to the boost direction, but now they exhibit some nontrivial isometry due to nontrivial holonomy induced by the moving particle.

To obtain the faces of the wedge of moving massive particle we make the boost, that in the matrix notation has the form:

$$\mathbf{u} = \cosh(\xi/2)\,\mathbf{1} - \sinh(\xi/2)\,\gamma_2 = \cosh(\xi/2)\,\mathbf{\Omega}(0) - \sinh(\xi/2)\,\mathbf{\Gamma}(\pi/2), \tag{2.9}$$

i.e. we apply (2.9) to the faces of the wedge (2.7) and (2.8) and get:

$$\mathbf{x}_{1-mov-face} = \mathbf{u}^{-1}\mathbf{x}_{1-face}\mathbf{u}, \quad \mathbf{x}_{2-mov-face} = \mathbf{u}^{-1}\mathbf{x}_{2-face}\mathbf{u}. \tag{2.10}$$

From (2.8) we find the isometry map identifying these two wedges:

$$\mathbf{x}_{2-nd\,mov\ face} = \mathbf{\Omega}_{\mathbf{u}}(\alpha/2, \xi/2)\ \cdot\ \mathbf{x}_{1-st\,mov\ face}\ \cdot\ \mathbf{\Omega}_{\mathbf{u}}(-\alpha/2, \xi/2), \tag{2.11}$$

where

$$\mathbf{\Omega}_{\mathbf{u}}(-\alpha/2, \xi/2) \equiv \mathbf{\Omega}_{\mathbf{u}} = \mathbf{u}^{-1}(\xi/2)\mathbf{\Omega}\,(-\alpha/2)\,\mathbf{u}(\xi/2).$$

Finally the isometry induced by the presence of the moving massive particle in AdS_3 is:

$$\mathbf{x}^* = \mathbf{\Omega}_{\mathbf{u}}^{-1}\mathbf{x}\mathbf{\Omega}_{\mathbf{u}} = \begin{pmatrix} x_3^* + x_2^* & x_0^* + x_1^* \\ x_1^* - x_0^* & x_3^* - x_2^* \end{pmatrix}, \tag{2.12}$$

where $\mathbf{x}$ is the AdS_3 point defined as (2.3).

Rewriting (2.3) in an explicit form using barrel coordinates:

$$\mathbf{x} = \begin{pmatrix} \cos t \cosh\chi + \sin\phi \sinh\chi & \cosh\chi \sin t + \cos\phi \sinh\chi \\ -\cosh\chi \sin t + \cos\phi \sinh\chi & \cos t \cosh\chi - \sin\phi \sinh\chi \end{pmatrix},$$

and (2.12) has the form:

$$\mathbf{x}^* = \begin{pmatrix} \cos t^* \cosh\chi^* + \sin\phi^* \sinh\chi^* & \cosh\chi^* \sin t^* + \cos\phi^* \sinh\chi^* \\ -\cosh\chi^* \sin t^* + \cos\phi^* \sinh\chi^* & \cos t^* \cosh\chi^* - \sin\phi^* \sinh\chi^* \end{pmatrix}.$$

After some algebra we get an explicit coordinate expression for isometry as:

$$\begin{aligned} \tan t^* &= \mathcal{B}_\xi(\alpha) \sec t \tanh\chi \cos\phi + \tan t \left(1 + 2\sinh^2\xi \sin^2\frac{\alpha}{2}\right), \\ \tan\phi^* &= -2\xi(\alpha)^{-1} \tan\phi, \end{aligned} \tag{2.13}$$

$$\cosh\chi^* = \cosh\chi[\left(\mathcal{B}_\xi(\alpha) \tanh\chi \cos\phi + \sin t(1 + 2\sinh^2\xi \sin^2\frac{\alpha}{2})\right)^2 + \cos^2 t]^{\frac{1}{2}},$$

where

$$\begin{aligned}\mathcal{B}_\xi(\alpha) &= \sinh\xi\left(\sin\alpha\tan\phi - 2\cosh\xi\sin^2\frac{\alpha}{2}\right), \\ \xi(\alpha) &= \cosh\xi(2\sin\alpha\tan\phi - \cos\alpha + \cos\phi) \\ &+ \sec\phi\cos(\alpha+\phi) + \cos\alpha\cosh 2\xi - 2\sinh^2\xi.\end{aligned} \tag{2.14}$$

From (2.13) taking the limit $\chi \to \infty$ we get the expression for isometry near the boundary of the AdS_3:

$$\begin{aligned}\tan t_b^* &= \mathcal{B}_\xi(\alpha)\sec t_b\cos\phi_b + \tan t_b\left(1 + 2\sinh^2\xi\sin^2\frac{\alpha}{2}\right), \\ \tan\phi_b^* &= -2\xi(\alpha)^{-1}\tan\phi_b.\end{aligned} \tag{2.15}$$

The expression for the radial coordinate χ after the isometry near the boundary is:

$$\mathrm{e}^{\chi_{nb}^*} = \mathrm{e}^{\chi_{nb}}\sqrt{\mathcal{A}}, \tag{2.16}$$

where

$$\mathcal{A} = \left(\mathcal{B}_\xi(\alpha)\cos\phi_b + \sin t_b(1 + 2\sinh^2\xi\sin^2\frac{\alpha}{2})\right)^2 + \cos^2 t_b.$$

Now we derive equations defining the wedge faces. As it has been mentioned above, to fix the wedges we must find points that are constant in time and symmetrical in angle under the isometry, i.e. they are fixed by conditions $t^* = t$ and $\phi^* = -\phi$. So, solving equation $\tan t = \tan t^*$ we get the expression for the wedge face:

$$\tanh\chi = \frac{2\sin t\sinh\xi\sin^2\frac{\alpha}{2}}{2\cosh\xi\sin^2\frac{\alpha}{2}\cos\phi \pm \sin\alpha\sin\phi}. \tag{2.17}$$

It is useful to change the variable as $r = \tanh(\chi/2)$ and get r as function of ϕ and t for two wedges:

$$r(\phi, t) = \tanh\left(\frac{1}{2}\mathrm{arctanh}\frac{2\sin t\sinh\xi\sin^2\frac{\alpha}{2}}{2\cosh\xi\sin^2\frac{\alpha}{2}\cos\phi \pm \sin\alpha\sin\phi}\right). \tag{2.18}$$

The intersection of two surfaces determined by (2.18) gives a fixed point of the isometry (or equally the massive particle worldline):

$$r(t) = \frac{1 - \sqrt{1 - \tanh^2\xi\sin^2 t}}{\tanh\xi\sin t}.$$

The massive particle moves from the left to right and vice versa periodically (with period $T = 2\pi$). Note that if $\xi \to \infty$ we will obtain the case of massless moving particle $r = \tan(t/2)$ that coincides with formulas for the massless particle in paper [35]. For constant time t slices the wedge faces are some curves intersecting

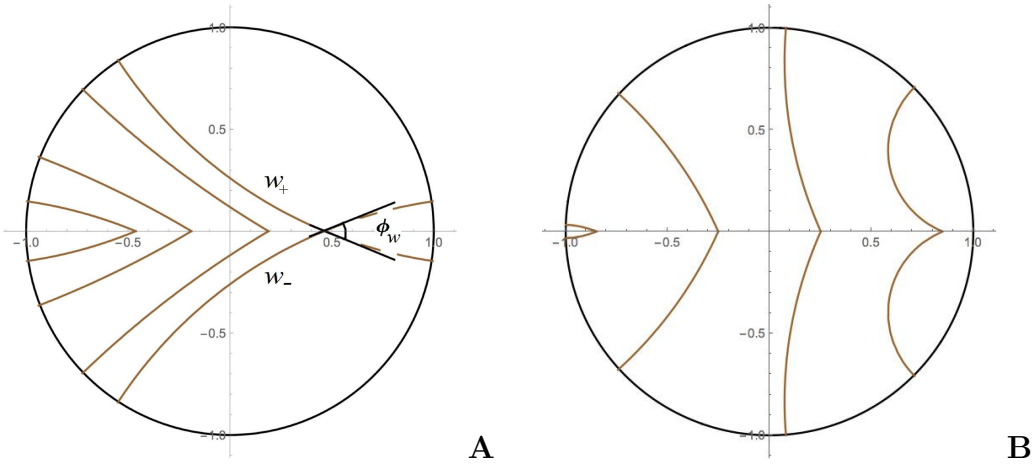

Figure 2. Constant time slices of the AdS_3 with a moving massive particle for different times. The black circle represents the boundary of the AdS_3 space and brown curves are sections of the faces of the wedge in different time moments: $t = -\pi/2, -0.5, 0.5$ and $\pi/2$ from the left to the right for the each plot. The section at $t = \pi/2$ of the wedge faces is indicated by $w_\pm$ and φ is the angle between $w_\pm$ at the crossing point, the location of the particle at $t = \pi/2$. We take parameter values to be $\xi = 1$, $\alpha = \pi/4$ (A) and to be $\xi = 2.5$, $\alpha = \pi/4$ (B).

at the particle position. The angle ϕ_w between these two curves at the intersection point can be expressed as:

$$\varphi = \arctan\left(\frac{4\sin^2\frac{\alpha}{2}\sin\alpha\cosh\xi\sqrt{1-\sin^2 t\tanh^2\xi}}{\sin^2\alpha - 4\sin^4\frac{\alpha}{2}\left(1+2\sinh^2\xi\sin^2\frac{\alpha}{2}\right)}\right).$$

From this formula we can see, that the angle ϕ_w is maximal at $t = \pm\frac{\pi}{2}$ if $\alpha > \pi$ and at $t = 0$ if $\alpha < \pi$ (see Fig.2).

Three dimensional plots of the wedge are presented in Fig.3.

2.3 Correlation functions on the boundary and geodesics in the AdS_3.

In the AdS/CFT correspondence, to calculate the two-point correlation function of a scalar operator Φ_Δ with large conformal weight Δ on the AdS_3 boundary, one can use the geodesic approximation [29]. In this approximation one defines the correlator:

$$G_\Delta(\phi_a, t_a; \phi_b, t_b) = e^{-\Delta\mathcal{L}_{ren}(\phi_a,t_a;\phi_b,t_b)}. \tag{2.19}$$

Here a and b are two points on the boundary of the AdS_3 with coordinates (ϕ_a, t_a) and (ϕ_b, t_b). For the spacelike separated points a and b, $\mathcal{L}_{ren}(\phi_a, t_a; \phi_b, t_b)$ is the renormalized length of the geodesic connecting these points [29, 30]. If a and b are timelike separated points, there is no geodesic between them. In the paper we restrict ourselves to the geodesics between spacelike-separated points. The contribution of

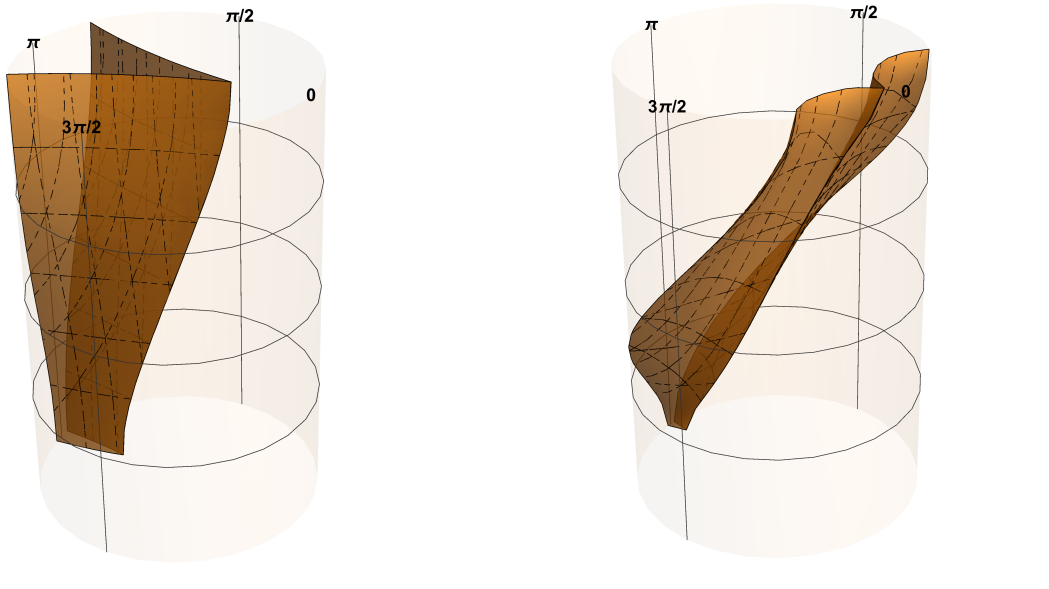

A **B**

Figure 3. The plot of the wedge of moving massive particle with certain parameters ξ and α values. Here $-\pi/2 < t < \pi/2$. A. Here we take parameter values to be $\xi = 1$, $\alpha = \pi/8$. B. Here we take parameter values to be $\xi = 2.5$, $\alpha = \pi/4$

timelike separated points from the geodesic prescription is considered in the next paper.

2.3.1 Spacelike separated points

Now we remind how the geodesic approximation works in the AdS_3 global coordinates. We consider two spacelike separated boundary points (ϕ_a, t_a) and (ϕ_b, t_b). We assume for definiteness $\phi_b > \phi_a$. The geodesic curve in the bulk $(\phi, t, r) = (\phi(\lambda), t(\lambda), r(\lambda))$, connecting these points is given by :

$$\phi_{ab}(\lambda) = \arctan\left(\tan\frac{D_s[\phi_a,\phi_b]}{2}\cdot\tanh\lambda\right) + \Sigma_s[\phi_a,\phi_b], \tag{2.20}$$

$$t_{ab}(\lambda) = \arctan\left(\tan\frac{D[t_a,t_b]}{2}\cdot\tanh\lambda\right) + \Sigma[t_a,t_b] \tag{2.21}$$

and

$$r(\lambda) = \frac{\sqrt{\cos(2D[t_a,t_b]+\cosh(2\lambda)} - \sqrt{\cos(2D[t_a,t_b]-\cos(2D_s[\phi_a,\phi_b]))}}{\sqrt{\cos(2D_s[\phi_a,\phi_b])+\cosh(2\lambda)}}.$$

Here the parametrization is taken so that the parameter value $\lambda = -\infty$ corresponds to the point (ϕ_a, t_a) on the boundary and $\lambda = +\infty$ corresponds to the point (ϕ_b, t_b).

$D_s[\phi_a,\phi_b]$, $D[t_a,t_b]$, $\Sigma_s[\phi_a,\phi_b]$ and $\Sigma[t_a,t_b]$ are defined as

$$\begin{aligned}
\phi_b-\phi_a<\pi: \quad D_s[\phi_a,\phi_b] &= \phi_b-\phi_a, \\
\Sigma_s[\phi_a,\phi_b] &= \frac{\phi_b+\phi_a}{2}; \\
\phi_b-\phi_a>\pi: \quad D_s[\phi_a,\phi_b] &= \phi_b-\phi_a-2\pi, \\
\Sigma_s[\phi_a,\phi_b] &= \frac{\phi_b+\phi_a}{2}+\pi; \\
D[t_a,t_b] &= t_b-t_a, \\
\Sigma[t_a,t_b] &= \frac{t_b+t_a}{2}.
\end{aligned} \tag{2.22}$$

Note, that in [33] another parametrization for this geodesic has been used.

It is easy to calculate the geodesic length $\mathcal{L}_{AdS}$ between two points on the curve (2.20)-(2.21) using

$$\begin{aligned}
\cosh\mathcal{L}_{AdS} &= -\frac{1}{2}\left[\det(\mathbf{x}_a-\mathbf{x}_b)-2\right] \\
&= -(x_{(a)},x_{(b)}) = x_{0,a}x_{0,b}+x_{3,a}x_{3,b}-x_{1,a}x_{1,b}-x_{2,a}x_{2,b},
\end{aligned} \tag{2.23}$$

where $x_{i,a}$ and $x_{i,b}$, $i=0,1,2,3$ are embedding coordinates (2.2) of the endpoints. Writing down (2.23) explicitly in coordinates (ϕ,t,χ) we express the geodesic length between points $a=(\phi_a,t_a,\chi_a)$ and $b=(\phi_b,t_b,\chi_b)$ as:

$$\begin{aligned}
&-\cosh\mathcal{L}(a;b) = \\
&= -\cosh\chi_a\,\sin t_a\cosh\chi_b\,\sin t_b-\cosh\chi_a\,\cos t_a\cosh\chi_b\,\cos t_b \\
&+\sinh\chi_a\,\cos\phi_a\sinh\chi_b\,\cos\phi_b+\sinh\chi_a\sin\phi_a\sinh\chi_b\sin\phi_b.
\end{aligned} \tag{2.24}$$

When points a and b go to the boundary (i.e. $\chi_{a,b}\to\infty$) one gets:

$$\begin{aligned}
\mathcal{L}_{reg}(a;b) &= \ln\left[(\cos(t_a-t_b)-\cos(\phi_a-\phi_b))\,\frac{e^{\chi_a+\chi_b}}{2}\right] \\
&= \ln\left[2(\cos(t_a-t_b)-\cos(\phi_a-\phi_b))\right]+\delta_a+\delta_b,
\end{aligned} \tag{2.25}$$

where $\delta_a=\chi_a-\ln 2$ and $\delta_b=\chi_b-\ln 2$.

Removing the divergent parts δ_a, δ_b in (2.25) we get the renormalized geodesic length for the spacelike geodesic connecting two points on the boundary:

$$\mathcal{L}_{ren}(t_a,\phi_a;t_b,\phi_b)=\ln[2\,(\cos(t_a-t_b)-\cos(\phi_a-\phi_b))], \tag{2.26}$$

From this formula and (2.19) the two-point function on the AdS_3 boundary is:

$$G_{\Delta,AdS}\,(\phi_a,t_a,\phi_b,t_b)=\left(\frac{1}{2(\cos(t_a-t_b)-\cos(\phi_a-\phi_b))}\right)^{\Delta}. \tag{2.27}$$

2.3.2 Timelike separated points

Mentioned above, there are no continous geodesics in the AdS_3 connecting two timelike separated points on the boundary. So, to use the geodesic approximation in calculation of two-point functions for timelike separated points, we use the prescription proposed in [30, 33]. This prescription is related with the prescription that has been early proposed in [11] in the Poincare patch. According to this prescription to calculate the correlator for timelike separated points one has to relate these points by a quasigeodesic, that consists of two pieces of the spacelike geodesics with a discontinuity at the Poincare horizon. The explicit formulae are

$$\phi_{ab}(\lambda) = \arctan\left(\tan\frac{D[\phi_a,\phi_b]}{2}\cdot\coth\lambda\right) + \Sigma[\phi_a,\phi_b], \tag{2.28}$$

$$t_{ab}(\lambda) = \arctan\left(\tan\frac{D[t_a,t_b]}{2}\cdot\coth\lambda\right) + \Sigma[t_a,t_b], \tag{2.29}$$

and

$$r(\lambda) = \frac{\sqrt{\cos(2D[t_a,t_b])+\cosh(2\lambda)} - \sqrt{\cos(2D[t_a,t_b])-\cos(2D[\phi_a,\phi_b])}}{\sqrt{\cos(2D[\phi_a,\phi_b]))+\cosh(2\lambda)}}, \tag{2.30}$$

where $D[t_a,t_b]$ and $\Sigma[t_a,t_b]$ are defined as (2.22)

In Fig.4 we plot the quasigeodesic corresponding to the boundary points a and b with coordinates (ϕ_a,t_a) and (ϕ_b,t_b), respectively.

For simplicity we consider the case of symmetric points. In this case the boundary points are taken to be $(\delta\phi,\delta t)$, $(-\delta\phi,-\delta t)$, where

$$\delta\phi = \frac{\phi_a-\phi_b}{2}, \qquad \delta t = \frac{t_a-t_b}{2}. \tag{2.31}$$

The part of the quasigeodesic that starts at the point a at $\lambda=-\infty$ reaches the Poincare horizon at the point with coordinates $(\phi_{h_1},t_{h_1},\chi_{h_1})$. These coordinates correspond to the values of the right hand side of formulae (2.28)-(2.30) at $\lambda\to-0$:

$$t_{h_1} = -\frac{\pi}{2}, \quad \phi_{h_1} = -\frac{\pi}{2}, \quad \chi_{h_1} = \operatorname{arcsinh}\frac{|\sin\delta\phi|}{\sqrt{\sin^2\delta t-\sin^2\delta\phi}}.$$

The part of the quasigeodesic that reaches the point b at $\lambda=+\infty$ starts from the Poincare horizon at the point with coordinates $(\phi_{h_2},t_{h_2},\chi_{h_2})$, that correspond to the values of the right hand side of formulae (2.28)-(2.30) at $\lambda\to+0$:

$$t_{h_2} = \frac{\pi}{2}, \quad \phi_{h_2} = \frac{\pi}{2}, \quad \chi_{h_2} = \operatorname{arcsinh}\frac{|\sin\delta\phi|}{\sqrt{\sin^2\delta t-\sin^2\delta\phi}}.$$

Taking $b=h_1$ and $a=a_r$ in formula (2.24) we get the geodesic length between a_r, the point near the boundary (i.e. χ is large) with coordinates $(-\delta\phi,-\delta t,\chi)$ and

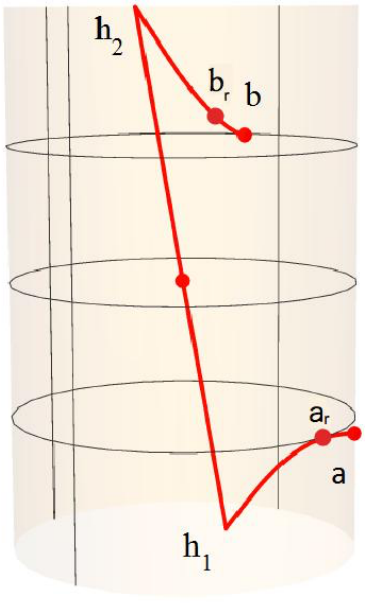

Figure 4. The plot of the quasigeodesic connecting two points a and b on the boundary. Points a and b correspond to affine parameter limits $\lambda \to \mp\infty$, respectively. Points a_r and b_r are the nearest points in the bulk corresponding to finite $\mp\lambda$ parameters. The curve ah_1 is the spacelike geodesic connecting the point a at the boundary and the point h_1 at the Poincare horizon. The curve ah_2 is the spacelike geodesic connecting the point b at the boundary and the point h_2 at the Poincare horizon.

the point h_1 with coordinates $(\phi_{h_1}, t_{h_1}, \chi_{h_1})$:

$$\mathcal{L}(a_r; h_1) = \ln\left(2\sqrt{\sin^2\delta t - \sin^2\delta\phi}\right) + \delta_{a_r} + ..., \quad \delta_{a_r} = \chi_{a_r} - \ln 2, \tag{2.32}$$

where dots mean subleading terms when $\chi \to \infty$. Subtracting the linear on χ term we get the renormalized geodesic length between the point a on the boundary and point h_1:

$$\mathcal{L}_{ren}(a; h_1) = \ln\left(2\sqrt{\sin^2\delta t - \sin^2\delta\phi}\right). \tag{2.33}$$

In a similar way taking $b = h_2$ and $a = b_r$ in formula (2.24) and subtracting the divergent term $\delta_{b_r} = \chi_{b_r} - \ln 2$ we get the renormalized geodesic length between the point b on the boundary and the point h_2 on the Poincare horizon:

$$\mathcal{L}_{ren}(b; h_2) = \ln\left(2\sqrt{\sin^2\delta t - \sin^2\delta\phi}\right). \tag{2.34}$$

Summing (2.33) and (2.34) we get

$$\begin{aligned}\mathcal{L}_{quasi,ren}(t_a, \phi_a; t_b, \phi_b) &= \mathcal{L}_{ren}(a; h_1) + \mathcal{L}_{ren}(b; h_2) \\ = 2\ln(2\sqrt{\sin^2\delta t - \sin^2\delta\phi}) &= \ln(2(-\cos(t_a - t_b) + \cos(\phi_a - \phi_b))),\end{aligned} \tag{2.35}$$

Combining (2.35) with the (2.19) we get the answer for the two-point correlation function for timelike separated points

$$G_{\Delta,AdS}\left(\phi_a, t_a, \phi_b, t_b\right) = \left(\frac{1}{2(-\cos(t_a - t_b) + \cos(\phi_a - \phi_b))}\right)^{\Delta}. \tag{2.36}$$

Comparing (2.27) and (2.36) we can write

$$G_{\Delta,AdS}\left(\phi_a, t_a, \phi_b, t_b\right) = \left(\frac{1}{2|\cos(t_a - t_b) - \cos(\phi_a - \phi_b)|}\right)^{\Delta}. \tag{2.37}$$

2.3.3 Reflection symmetry

As has been noted in [33] the correlator (2.37) possesses the reflection symmetry,

$$G_{\Delta,AdS}(\phi_a, t_a; \phi_b, t_b) = G_{\Delta,AdS}(\phi_a, t_a; \phi_b + \pi, t_b + \pi),$$

i.e. this correlator is invariant under a shift on π of both arguments t and ϕ simultaneously. The transformation $(t, \phi) \to (t + \pi, \phi + \pi)$ is the reflection transformation. Under this transformation the timelike interval ab transforms to the spacelike one ab'' and vice versa (see Fig.5).

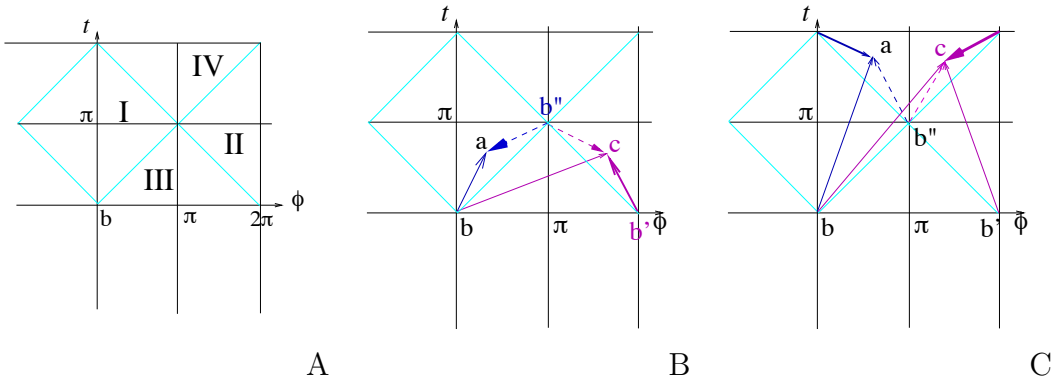

Figure 5. A. The plot shows different regions I, II, III and IV. Regions I and II are timelike regions with respect to the "trigonometrical" interval $-\cos(t_b - t_c) + \cos(\phi_b - \phi_c)$ for $t_b = 0$, $\phi_b = 0$. Regions III and IV are spacelike regions with respect to the "trigonometrical" interval. B. The plot of the reflection transformation in the parts of the region I (blue vectors) $\vec{ba} \to \vec{b''a}$, in the the region II (magenta vectors) $\vec{b'c} \to \vec{b''c}$, here $0 < t_a < \pi$. C. The plot of the reflection transformation $\vec{ba} \to \vec{b''a}$ and $\vec{bc} \to \vec{b''c}$ in the region IV.

2.3.4 Remarks about the Wightman, causal and retarded correlators

Let us note the relation of the function (2.37) defined via the geodesics approximation with the causal, retarded and Wightman correlators. The Wightman correlators are

obtained [38–40] by the $i\epsilon$ prescription from the CFT correlators on the Euclidean cylinder

$$G_E(\phi_a,\tau_a;,\phi_b,\tau_b)=\left(\frac{1}{2(\cosh(\tau_a-\tau_b)-\cos(\phi_a-\phi_b))}\right)^{\Delta}. \tag{2.38}$$

and can be written as

$$\begin{aligned} G_W(\phi_a,t_a;\phi_b,t_b) &= \langle O(\phi_a,t_a)O(\phi_b,t_b)\rangle \\ &= \left(\frac{1}{2(\cos(t_a-t_b-i\epsilon)-\cos(\phi_a-\phi_b))}\right)^{\Delta} \end{aligned} \tag{2.39}$$

In the sense of distributions [41] we can present (2.39) as

$$\begin{aligned} &G_W(\phi_a,t_a;\phi_b,t_b)=G_{\Delta,AdS}(\phi_a,t_a;\phi_b,t_b) \\ &\cdot\{\Psi_W(t_a;t_b)\,\theta(-\cos(t_a-t_b)+\cos(\phi_a-\phi_b)]+\theta(\cos(t_a-t_b)-\cos(\phi_a-\phi_b))\} \end{aligned} \tag{2.40}$$

where $G_{\Delta,AdS}$ is defined as (2.37) and Ψ_W function is:

$$\Psi_W(t_a;t_b)=e^{-i\,\pi\,\Delta\,\mathrm{sign}(\sin(t_a-t_b))}.$$

Using (2.39) one gets the representation for the causal correlator of the conformal fields on the cylinder:

$$\begin{aligned} G_c(\phi_a,t_a;\phi_b,t_b) &= \langle TO(\phi_a,t_a)O(\phi_b,t_b)\rangle_c \\ &= \left(\frac{1}{2(\cos(t_a-t_b-i\epsilon(t_a-t_b))-\cos(\phi_a-\phi_b))}\right)^{\Delta}, \end{aligned} \tag{2.41}$$

that can be written as

$$\begin{aligned} &G_c(\phi_a,t_a;\phi_b,t_b)=G_{\Delta,AdS}(\phi_a,t_a;\phi_b,t_b) \\ &\cdot\{\Psi_c(t_a;t_b)\,\theta(-\cos(t_a-t_b)+\cos(\phi_a-\phi_b))+\theta(\cos(t_a-t_b)-\cos(\phi_a-\phi_b))\}, \end{aligned} \tag{2.42}$$

where

$$\Psi_c(t_a;t_b)=e^{-i\,\pi\,\Delta\,\mathrm{sign}(\sin(t_a-t_b))}\,\theta(t_a-t_b)+e^{i\pi\,\Delta\,\mathrm{sign}(\sin(t_a-t_b))}\,\theta(-t_a+t_b).$$

The retarded correlator can be represented as

$$G_{ret}(\phi_a,t_a;\phi_b,t_b)\equiv\theta(t_a-t_b)\langle[O(\phi_a,t_a),O(\phi_b,t_b)]\rangle, \tag{2.43}$$

and then we have

$$\begin{aligned} &G_{\ ret}(\phi_a,t_a;\phi_b,t_b)= \\ &=G_{\Delta,AdS}(\phi_a,t_a;\phi_b,t_b)\Psi_{ret}(t_a;t_b)\cdot\,\theta(t_a-t_b)\theta(-\cos(t_a-t_b)+\cos(\phi_a-\phi_b)), \end{aligned}$$

where

$$\Psi_{ret}(t_a;t_b) = -2i\sin(\pi\Delta\,\mathrm{sign}(\sin(t_a-t_b))).$$

The above formula can be written in the universal way

$$G_{A,\Delta}(\phi_a,t_a;\phi_b,t_b) = G_{\Delta,AdS}(\phi_a,t_a;\phi_b,t_b)\cdot\Phi_{A,\Delta}(\phi_a,t_a;\phi_b,t_b),$$

where the subscript A means Wightman (W), causal (c) or retarded (r) and

$$\Phi_{B,\Delta}(\phi_a,t_a;\phi_b,t_b) = \tag{2.44}$$
$$= \Psi_{B,\Delta}(t_a;t_b)\cdot\theta(-\cos(t_a-t_b)+\cos(\phi_a-\phi_b))+\theta(\cos(t_a-t_b)-\cos(\phi_a-\phi_b))$$
$$\Phi_{ret,\Delta}(\phi_a,t_a;\phi_b,t_b) = \tag{2.45}$$
$$= \Psi_{ret,\Delta}(t_a;t_b)\cdot\theta(t_a-t_b)\theta(-\cos(t_a-t_b)+\cos(\phi_a-\phi_b)),$$

and where subscript B stands for Wightman (W) or causal (c).

For an integer Δ the functions defined by (2.44) and (2.42) coincide and the factor Ψ_{ret} is zero.

3 Image method and winding geodesics

3.1 Image method on the living space

When the AdS_3 is deformed by the point particle, formulae (2.39), (2.41) and (2.43) have to be modified. In particular,

$$< TO(\phi_a,t_a)O(\phi_b,t_b) >_{l.s.}= \tag{3.1}$$
$$= \left(\frac{1}{2(\cos(t_a-t_b+i(t_a-t_b)\epsilon)-\cos(\phi_a-\phi_b))}\right)^{\Delta}\Theta_0(\phi_a,t_a;\phi_b,t_b)$$
$$+\sum_{n\in Z}\left(\frac{1}{2(\cos(t^*_{a,n}-t_b+i(t^*_{a,n}-t_b)\epsilon)-\cos(\phi^*_{a,n}-\phi_b))}\right)^{\Delta}\Theta_n(\phi^*_{a,n},t^*_{a,n};\phi_b,t_b)Z_n(\phi^*_{a,n},t^*_{a,n};\phi_b,t_b)$$
$$+\sum_{n\in Z}\left(\frac{1}{2(\cos(t^{\#}_{a,n}-t_b+i(t^{\#}_{a,n}-t_b)\epsilon)-\cos(\phi^*_{a,n}-\phi_b))}\right)^{\Delta}\bar{\Theta}_n(\phi^{\#}_{a,n},t^{\#}_{a,n};\phi_b,t_b)\bar{Z}_n(\phi^{\#}_{a,n},t^{\#}_{a,n};\phi_b,t_b)$$

Here the subscript l.s. in the LHS of (3.1) means a living space of the boundary of the AdS_3 with static or moving defects and

$$(\phi_a,t_a)^{*\,n} = (\phi^*_{a,n},t^*_{a,n}),$$

are coordinates of the image points obtained by n-times applications of the isometry *-transformation (2.12). The #-transformation is defined so that

$$(\phi^{\#}_a\,t^{\#}_a)^* = (\phi_a,t_a),$$

and we also use notations

$$(\phi_a, t_a)^{\#\, n} = (\phi^{\#}_{a,n}, t^{\#}_{a,n}). \tag{3.2}$$

In comparison with the usual image formula for Green functions, see for example eq.(4.1.35) in [42], we put in (3.1) the extra factors:

$$\Theta_n(\phi^*_{a,n}, t^*_{a,n}; \phi_b, t_b), \quad \Theta_n(\phi^{\#}_{a,n}, t^{\#}_{a,n}; \phi_b, t_b),$$
$$Z_n(\phi^*_{a,n}, t^*_{a,n}; \phi_b, t_b), \quad \bar{Z}_n(\phi^{\#}_{a,n}, t^{\#}_{1,n}; \phi_b, t_b),$$

The first two factors take values 1 or 0, depending on a particular image contribution, see more explanations below. Factors Z and Z_n are related to renormalizations, see also below Sect.3.4.

According to (2.42) we have

$$\begin{aligned} &< TO(\phi_a, t_a)O(\phi_b, t_b) >_{l.s.}= \\ &= \Phi_{c,\Delta}(\phi_a, t_a; \phi_b, t_b) G_{\Delta,AdS}(\phi_a, t_a; \phi_b, t_b)\, \Theta_0(\phi_a, t_a; \phi_b, t_b) \\ &+ \sum_{n\in Z}^{n_{max}} \Phi_{c,\Delta}(\phi^*_{a,n}, t^*_{a,n}; \phi_b, t_b)\, G_{\Delta,AdS}(\phi^*_{a,n}, t^*_{a,n}; \phi_b, t_b)\, \Theta_n(\phi^*_{a,n}, t^*_{a,n}; \phi_b, t_b)\, Z_n(\phi^*_{a,n}, t^*_{a,n}; \phi_b, t_b) \\ &+ \sum_{n\in Z}^{\bar{n}_{max}} \Phi_{c,\Delta}(\phi^{\#}_{a,n}, t^{\#}_{a,n}; \phi_b, t_b)\, G_{\Delta,AdS}(\phi^{\#}_{a,n}, t^{\#}_{a,n}; \phi_b, t_b) \bar{\Theta}_n(\phi^{\#}_{a,n}, t^{\#}_{a,n}; \phi_b, t_b)\, \bar{Z}_n(\phi^{\#}_{a,n}, t^*_{a,n}; \phi_b, t_b) \end{aligned} \tag{3.3}$$

where $G_{\Delta,AdS}(\phi_a, t_a; \phi_b, t_b)$ is given by (2.37) and $\Phi_{c,\Delta}(\phi_a, t_a; \phi_b, t_b)$ by (2.44).

The presence of the Φ-factors in summands in (3.3) is related to the change of the causal relation between two points on the boundary under the isometry transformation (2.13). This is illustrated in Fig.6 and Fig.7.

In Fig.6 a schematic plot of geodesics connecting the points a_i, $i = 1, 2$ with $b = (0, 0)$ and $b^{\#}$ is presented. The coordinates of the point $b^{\#}$ is defined by the transformation (3.2). We see that originally spacelike separated points can keep their causal relation after the $*$ and $\#$ transformations and also can change their causal relation.

In Fig.7 a schematic plot of geodesics connecting the points a_i, $i = 1, 2$ with $b = (0, 0)$ and b^* is presented. The coordinates of the point b^* is defined by the transformation (2.12). We see that originally spacelike separated points can keep their causal relation as well, after the isometry $*$ transformation, can become timelike separated.

In this paper we ignore the contribution from timelike separated points, so we ignore Φ-factors and define

$$\begin{aligned} G_{l.s.}(\phi_a, t_a, \phi_b, t_b) &= G_{\Delta,AdS}(\phi_a, t_a; \phi_b, t_b)\, \Theta_0(\phi_a, t_a; \phi_b, t_b) \\ &+ \sum_n G_{\Delta,AdS}(\phi^*_{a,n}, t^*_{a,n}; \phi_b, t_b)\, Z_n(\phi^*_{a,n}, t^*_{a,n}; \phi_b, t_b)\, \Theta_n(\phi^*_{a,n}, t^*_{a,n}; \phi_b, t_b) \\ &+ \sum_n G_{\Delta,AdS}(\phi^{\#}_{a,n}, t^{\#}_{a,n}; \phi_b, t_b), \bar{Z}_n(\phi^{\#}_{a,n}, t^*_{a,n}; \phi_b, t_b) \bar{\Theta}_n(\phi^{\#}_{a,n}, t^{\#}_{a,n}; \phi_b, t_b) \end{aligned} \tag{3.4}$$

Absorbing Z-factors into the definition of $G_{\Delta,ren,n}(t^*_{a,n}, \phi^*_{a,n}; t_b, \phi_b)$

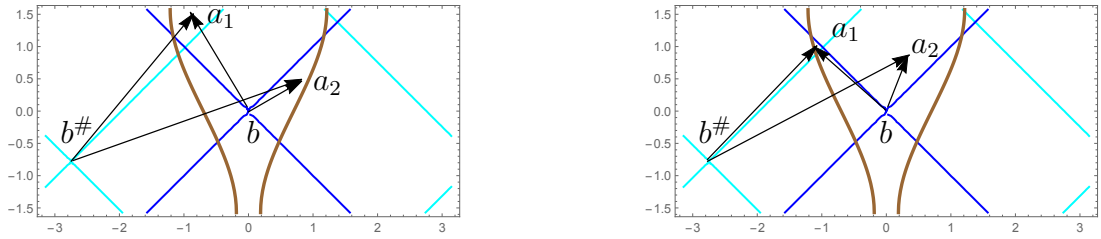

Figure 6. The schematic plot of geodesics connecting the points a_i, $i = 1, 2$ with points $b = (0, 0)$ and $b^{\#}$. A. The points b and a_1 are timelike separated and points $b^{\#}$ and a_1 are also timelike separated. The points b and a_2 are spacelike separated and also points $b^{\#}$ and a_2 are spacelike separated. B. The points b and a_1 are spacelike separated while points $b^{\#}$ and a_1 are also timelike separated. The points b and a_2 are timelike separated while points $b^{\#}$ and a_2 are spacelike separated. Here $\alpha = 1,\ \xi = 1$.

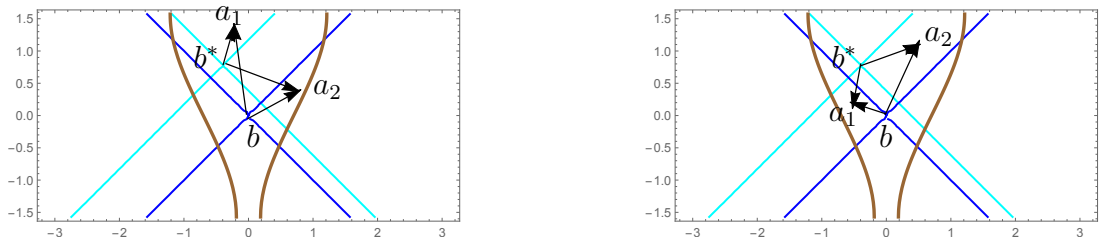

Figure 7. The schematic plot of geodesics connecting the points a_i, $i = 1, 2$ with $b = (0, 0)$ and b^*. A. The points b and a_1 are timelike separated and points b^* and a_1 are also timelike separated. The points b and a_2 are spacelike separated and points b^* and a_2 are also spacelike separated. B. The points b and a_1 are spacelike separated while points $b*$ and a_1 are timelike separated. The points b and a_2 are timelike separated while points b^* and a_2 are spacelike separated. Here $\alpha = 1,\ \xi = 1$.

$$
\begin{aligned}
G_{\Delta,ren,n}(\phi^*_{a,n}, t^*_{a,n}; \phi_b, t_b) &\equiv G_{\Delta,AdS}(\phi^*_{a,n}, t^*_{a,n}; \phi_b, t_b) Z_n(\phi^*_{a,n}, t^*_{a,n}; \phi_b, t_b) \\
G_{\Delta,ren,n}(\phi^{\#}_{a,n}, t^{\#}_{a,n}; \phi_b, t_b) &\equiv G_{\Delta,AdS}(\phi^{\#}_{a,n}, t^{\#}_{a,n}; \phi_b, t_b)\, \bar{Z}_n(\phi^{\#}_{a,n}, t^{\#}_{1,n}; \phi_b, t_b)
\end{aligned}
\tag{3.5}
$$

we get

$$
\begin{aligned}
G_{l.s.}(\phi_a, t_a, \phi_b, t_b) = {} & G_{\Delta,AdS}(\phi_a, t_a; \phi_b, t_b)\, \Theta_0(\phi_a, t_a; \phi_b, t_b) \\
& + \sum_n G_{\Delta,ren,n}(\phi^*_{a,n}, t^*_{a,n}; \phi_b, t_b)\, \Theta_n(\phi^*_{a,n}, t^*_{a,n}; \phi_b, t_b) \\
& + \sum_n G_{\Delta,ren,n}(\phi^{\#}_{a,n}, t^{\#}_{a,n}; \phi_b, t_b)\, \bar{\Theta}_n(\phi^{\#}_{a,n}, t^{\#}_{a,n}; \phi_b, t_b),
\end{aligned}
\tag{3.6}
$$

and in one keeps the isometry invariance in the renormalization prescription then the following properties take place:

$$G_{\Delta,ren,n}(\phi^*_{a,n},t^*_{a,n};\phi_b,t_b)=G_{\Delta,ren,n}(\phi^*_{a,n-1},t^*_{a,n-1};\phi^{\#}_{b,1},t^{\#}_{b,1})=G_{\Delta,ren,n}(\phi_a,t_a;\phi^{\#}_{b,n},t^{\#}_{b,n})$$
$$G_{\Delta,ren,n}(\phi^{\#}_{a,n},t^{\#}_{a,n};\phi_b,t_b)=G_{\Delta,ren,n}(\phi^{\#}_{a,n-1},t^{\#}_{a,n-1};\phi^*_{b,1},t^*_{b,1})=G_{\Delta,ren,n}(\phi_a,t_a;\phi^*_{b,n},t^*_{b,n}).$$

In formulae (3.4) and (3.6) we do not specify ranges of summation over n. We clarify ranges of summation for static defect in Sect.3.2 and for moving defect in Sect.3.3. As has been noted in Sect.2.3 the function $G_{\Delta,AdS}(\phi_a,t_a;\phi_b,t_b)$ is related with the renormalized geodesic lengths. The function $G_{\Delta,ren,n}(\phi^*_{a,n},t^*_{a,n};\phi_b,t_b)$ also is related with renormalized geodesic lengths for the cases when geodesics cross the wedge, see Sect.3.4 Therefore, we can shortly write

$$G_{l.s.}(\phi_a,t_a;\phi_b,t_b)=\sum e^{-\Delta\mathcal{L}_{ren}(\phi_a,t_a;\phi_b,t_b)}. \tag{3.7}$$

Here the sum is over all geodesics connecting the points a and b with coordinates $(\phi_a,t_a),(\phi_b,t_b)$ that belong to the living space of the AdS_3 with a wedge. The presence of Θ-functions is implicitly assumed and summation only over geodesics with $\Theta=1$ is relevant. These geodesic configurations can be different for different points choice and characteristics of moving particles.

In Sect.3.3 we consider representation (3.7) for the AdS_3 with one moving defect. To make our presentation more clear we start from one static defect, Sect.3.2.

3.2 Static defect.

In this section we formulate the renormalized image method of counting and calculation of geodesic contributions in the right hand side of formula (3.7) for the AdS_3 with one static defect. This case has been considered in the previous papers [29] for spacelike separated points and in [30, 33] for timelike separated points. We start from this case to set the notations and to describe our general method in a simpler case.

3.2.1 Equal-time points.

Now we formulate the image method for the case of one static defect and for equal-time points. Our prescription for calculation gives:

$$\begin{aligned}G_{l.s}\left(\phi_a,t_a,\phi_b,t_a\right)&=G_{\Delta,AdS}\left(\phi_a,t_a,\phi_b,t_a\right)\\&+\sum_{n=1}^{n=n_{max}}G_{\Delta,ren,n}\left(\phi_a,t_a,\phi_{b^{\star n}},t_a\right)+\sum_{n=1}^{n=\bar{n}_{max}}G_{\Delta,ren,n}\left(\phi_a,t_a,\phi_{b^{\#n}},t_a\right).\end{aligned} \tag{3.8}$$

Let us make a few comment about this formula. According to this formula to calculate the correlator we have to take into account:

- contribution from the basic geodesic connecting points a and b;
- contributions from the geodesics connecting a and all imaginary points $b^{\star\, n}$ of b,

$$b^{*\, n} \equiv b^{\underbrace{*\ldots*}_{n}}$$

that lie in the right from a half circle, i.e.

$$|\phi_a - \phi_{b^{*\, n}}| < \pi, \quad n \leq n_{max} \tag{3.9}$$

- contributions from the geodesics connecting A and all imaginary points $b^{\#\, n}$ of b,

$$b^{\#\, n} = b^{\underbrace{\#\ldots\#}_{n}}$$

lying in the left from a half circle i.e.

$$|\phi_a - \phi_{b^{\#\, n}}| < \pi, \quad n \leq \bar{n}_{max}. \tag{3.10}$$

More explicitly our prescription has the form:

$$\begin{aligned} &G_{l.s.}\left(\phi_a, t_a, \phi_b, t_a\right) = G_{\Delta, AdS}\left(\phi_a, t_a, \phi_b, t_a\right) \\ &+ \sum_{n=1}^{n=n_{max}} G_{\Delta, AdS}\left(\phi_a, t_a, \phi_b + n\bar{\alpha}, t_a\right) + \sum_{n=1}^{n=\bar{n}_{max}} G_{\Delta, AdS}\left(\phi_a, t_a, \phi_b - n\bar{\alpha}, t_a\right), \end{aligned} \tag{3.11}$$

where $\bar{\alpha} = 2\pi - \alpha$, n_{max} and $\bar{n}_{max}$ are given by (3.9) and (3.10). In the case $\alpha < \pi$ we have only one image point and the presence of the contribution of the additional geodesic depends on position of the points a and b, see [30]. For the case $\alpha > \pi$ we can get several terms in (3.11).

In Fig.8.A the contributions of additional geodesics are shown. The geodesics connect the point a with 3 image points obtained by the counterclockwise rotation of the point b on the angle $\bar{\alpha}$, $2\bar{\alpha}$ and $3\bar{\alpha}$, respectively. Only 3 geodesics ab, ab^* and ab^{**} contribute for the given position of the points a and b. The geodesic ab^{***} does not contribute since b^{***} is out of the right semi circle indicated by the red line. In the Fig.9.A contributions of additional geodesics are shown. The geodesics connect the point a and the imaginary point $b^{\#}$, obtained by the clockwise rotation on the angle $\bar{\alpha}$ of the point b, can be represented as a sum of two geodesics . The contributions can be represented as the sum of two geodesics. The first geodesic connects the point a with a point on the wedge, the point K, and the second one connects the point $K^{\#}$, the image of the point K, with the point b. One can seen that the geodesics $ab^{\#\#}$ and $ab^{\#\#\#}$ do not contribute since its length corresponds to a connection of the point a with the point b' that is not the image of b. Fig.8.B and Fig.9.B show the role of restrictions (3.9) and (3.10).

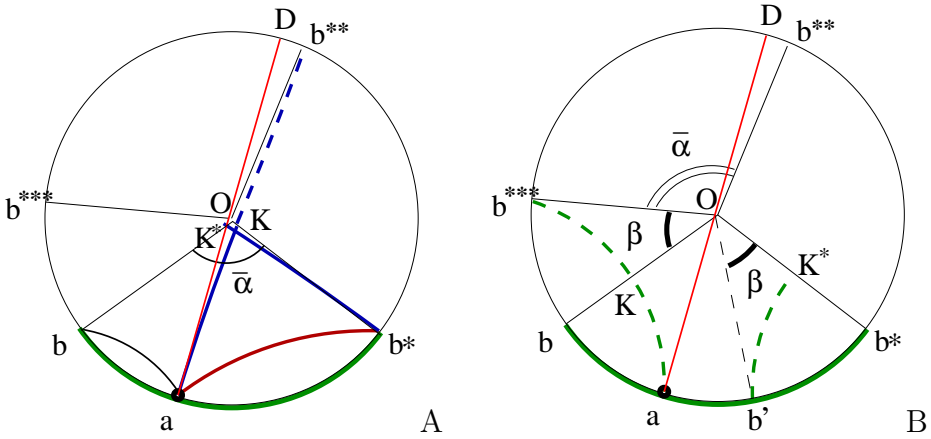

Figure 8. Plots of geodesics connecting the point a with 3 image points b^*, b^{**} and b^{***} (A). The contribution of the ab^{***} corresponds to the connection of the points a and b' (B).

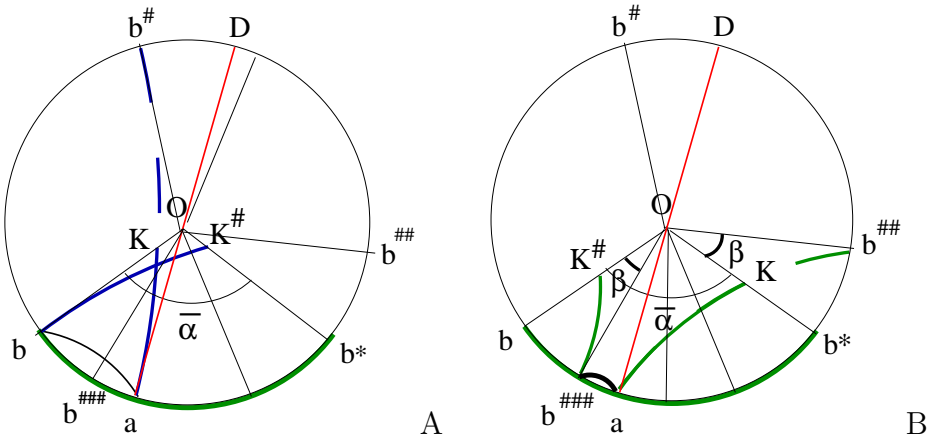

Figure 9. Plots of geodesics connecting the point a with 3 image points $b^{\#}$, $b^{\#\#}$ and $b^{\#\#\#}$ (A). Imaginary points $b^{\#\#}$ and $b^{\#\#\#}$ are out of the left semi circle indicated by the red line (B).

3.2.2 Proof of periodicity

To proof that (3.11) defines the correlator on the circle, we have to check that

$$G_{l.s.}\left(\phi_a, t_a, \phi_b, t_a\right) = G_{l.s.}\left(\phi_a, t_a, \phi_b + \bar{\alpha}, t_a\right). \tag{3.12}$$

Let us consider a particular case presented in Fig.10.A. For this case there are the following contributions to the LHS of (3.12): the contribution from the geodesic connecting the points a and b (the basic geodesic), then the contributions from geodesics connecting the point a with the image points b^*, b^{**} and $b^{\#}$, i.e. in (3.9), (3.10) $n_{max} = 2$, $\bar{n}_{max} = 1$.

To calculate the RHS of (3.12) we note that after the shift $\phi_b \to \phi_b + \bar{\alpha}$ according to our prescription there are the following contributions. There is the contribution from the basic geodesic between points pair (a, c), here we denote the point with coordinates $(\phi_b + \bar{\alpha}, t_a)$ as c (see Fig.10 B). There are also contributions from the image geodesics between points pairs (a, c^*) that is the same as (a, b^{**}), $(a, c^{\#})$ that is the same as (a, b) and $(a, c^{\#\#})$ that is the same as $(a, b^{\#})$, i.e. n_{max} and $\bar{n}_{max}$ are changed so that $n_{max} = 1$, $\bar{n}_{max} = 2$ (see Fig.10 B). Therefore the changes of n_{max} and $\bar{n}_{max}$ after the shift on the period preserves the set of contributing geodesics, that makes $G_{l.s.}$ periodic.

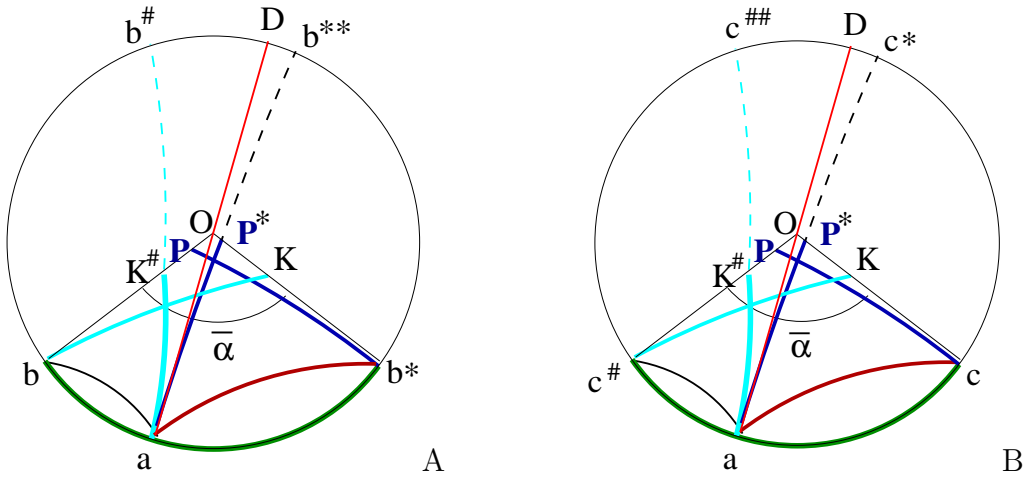

Figure 10. A. Plots of geodesics connecting points a and b, $b^{\#}$, b^{**}. B. Plots of geodesics connecting points a and c (where $\phi_c = \phi_b + \bar{\alpha}$), $c^{\#}$, c^*, $c^{\#\#}$.

3.2.3 Spacelike separated points

Our rule of construction the correlators for two spacelike separated points in the presence of the static defect is the same as for equal-time points:

$$G_{l.s.}(\phi_a, t_a, \phi_b, t_b) = G_{\Delta,AdS}(\phi_a, t_a, \phi_b, t_b) + \sum_{n=1}^{n=n_{max}} G_{\Delta,AdS}(\phi_a, t_a, \phi_b + n\bar{\alpha}, t_b) + \sum_{n=1}^{n=\bar{n}_{max}} G_{\Delta,AdS}(\phi_a, t_a, \phi_b - n\bar{\alpha}, t_b), \tag{3.13}$$

where n_{max} and $\bar{n}_{max}$ are found from restrictions (3.9) and (3.10). A schematic picture for different contributions to the right hand side of (3.13) is presented in Fig.11.

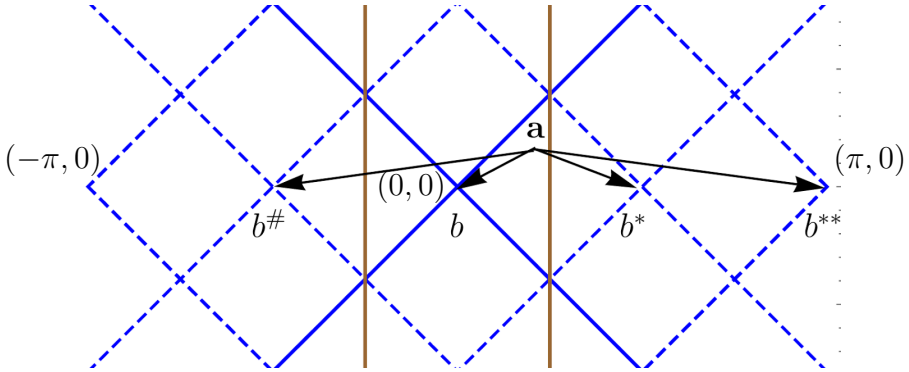

Figure 11. The schematic plot of geodesics connecting the spacelike separated points a and $b = (0, 0)$ and the point a with images of the point b: $b^* = (0, \bar{\alpha})$, $b^{**} = (0, 2\bar{\alpha})$, $b^{\#} = (0, -\bar{\alpha})$. Here $\alpha = 3\pi/2$.

3.2.4 Universal formula and isometry invariance

If we have the invariance of G_{ren} under the isometry related with the defect

$$G_{ren}\left(\phi_a, t_a, \phi_b - \bar{\alpha}, t_b\right) = G_{l.s.}\left(\phi_a + \bar{\alpha}, t_a, \phi_b, t_b\right), \tag{3.14}$$

then we can rewrite formula (3.13) in the form

$$\begin{aligned} G_{ren}\left(\phi_a, t_a, \phi_b, t_b\right) = {} & G_{\Delta,AdS}\left(\phi_a, t_a, \phi_b, t_b\right)\Theta_0(\phi_a, t_a, \phi_b, t_b) \\ & + \sum_{n=1}^{n=n_{max}} G_{\Delta,AdS}\left(\phi_a, t_a, \phi_b + n\bar{\alpha}, t_b\right) + \sum_{n=1}^{n=\bar{n}_{max}} G_{\Delta,AdS}\left(\phi_a + n\bar{\alpha}, t_a, \phi_b, t_b\right). \end{aligned} \tag{3.15}$$

3.3 Moving particle.

In this section we consider the two-point correlator of operators on the boundary in the presence of moving defect in the bulk.[1] Now we have a fixed direction that specifies the defect movement. We choose the coordinate system according to Fig.2.The isometry is given by formulae (2.15).

For moving massive particle the analog of formula (3.6) is

[1]If we consider on massive particle, then we can make Lorentz transformation to switch to a reference frame, where the particle is static. Then the problem that is under consideration in Sec3.3 reduces to problem from Sec.3.2. Nevertheless, we consider massive moving in laboratory frame, taking into account future generalization to the multiple particles case [43].

$$G_{l.s.}\left(\phi_a,t_a,\phi_b,t_b\right)=G_{\Delta,AdS}\left(\phi_a,t_a,\phi_b,t_b\right)\Theta_0(\phi_a,t_a;\phi_b,t_b;\alpha,\xi) \tag{3.16}$$
$$+\sum_{n=1}^{n=n_{max}} G_{\Delta,ren,n}\left(\phi_a^{\#n},t_a^{\#n},\phi_b,t_b\right)\Theta_{cr}(\phi_a^{\#n},t_a^{\#n};\phi_b,t_b;\alpha,\xi)$$
$$+\sum_{n=1}^{n=\bar{n}_{max}} G_{\Delta,ren,n}\left(\phi_a^{*n},t_a^{*n},\phi_b,t_b\right)\Theta_{cr}(\phi_a^{*n},t_a^{*n};\phi_b,t_b;\alpha,\xi),$$

where n_{max} and $\bar{n}_{max}$ are given by (3.9) and (3.10), i.e. they are as in the static case. The renormalizations defined $G_{\Delta,ren,n}$ are assumed to respect isometry (2.15) and we elaborate on this issue in the Sect.3.4. In (3.16) we introduce functions $\Theta_0(\phi_a,t_a;\phi_b,t_b;\alpha,\xi)$ and $\Theta_{cr}(\phi_a,t_a;\phi_b,t_b;\alpha,\xi)$ defined below.

The function Θ_0 is defined as:

- $\Theta_0(\phi_a,t_a;\phi_b,t_b;\alpha,\xi)=1$ if geodesic connecting points (ϕ_a,t_a) and (ϕ_b,t_b) does not cross the wedge;
- $\Theta_0(\phi_a,t_a;\phi_b,t_b;\alpha,\xi)=0$ if geodesic connecting points (ϕ_a,t_a) and (ϕ_b,t_b) crosses the wedge.

Θ_{cr} ("cr" means "crossing") is defined as following:

- $\Theta_{cr}(\phi_a,t_a;\phi_b,t_b;\alpha,\xi)=1$ if geodesic connecting (ϕ_a,t_a) and (ϕ_b,t_b) crosses the face w_- of the wedge;
- $\Theta_{cr}(\phi_a,t_a;\phi_b,t_b;\alpha,\xi)=0$ if geodesic connecting (ϕ_a,t_a) and (ϕ_b,t_b) does not cross the face w_- of the wedge (see Fig.2).

3.3.1 Light moving massive particle

For the case $\alpha<\pi$ there are only two terms in (3.16), one contribution comes from the "basic" geodesic, another two come from its images:

$$\begin{aligned}G_{\alpha,\xi}(\phi_a,t_a,\phi_b,t_b)&=G_{\Delta,AdS}\left(\phi_a,t_a,\phi_b,t_b\right)\Theta_0(\phi_a,t_a;\phi_b,t_b;\alpha,\xi)\\&+G_{\Delta,ren,1}(\phi_{a^*},t_{a^*},\phi_b,t_b)\,\Theta_{cr}(\phi_{a^*},t_{a^*};\phi_b,t_b;\alpha,\xi)\\&+G_{\Delta,ren,1}(\phi_a,t_a,\phi_{b^*},t_{b^*})\,\Theta_{cr}(\phi_a,t_a;\phi_{b^*},t_{b^*};\alpha,\xi).\end{aligned} \tag{3.17}$$

Finding support of functions Θ_0 and Θ_{cr} numerically we get different possibilities for the geodesic structure. We call the basic geodesic the geodesic that connects two points a and b on the boundary without crossing the wedge. We call winding or image geodesic the one that starting from the boundary meets the wedge at a point, comes out from it at the image point and reaches the boundary. !!!!!! In particular

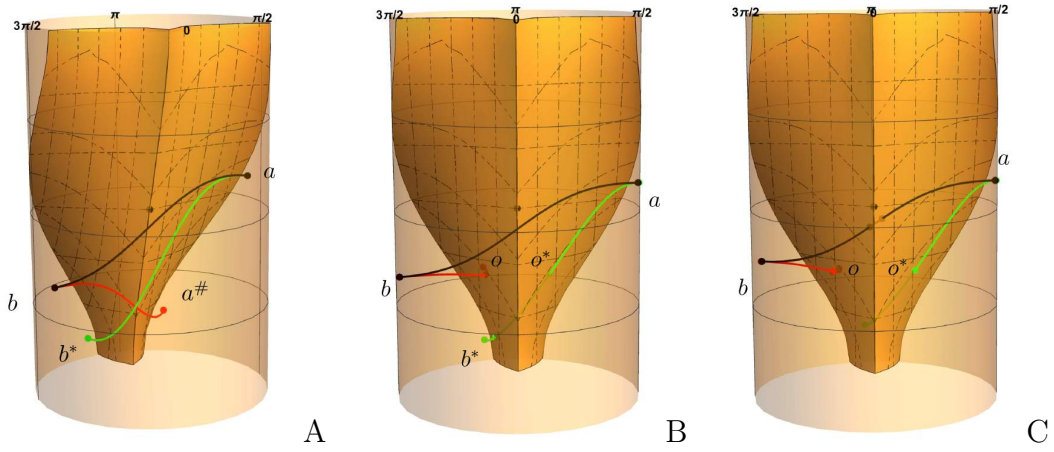

Figure 12. The plot of the wedge and geodesic configurations for the light particle. The black curves are the basic geodesics between points a and b. The red and green curves are the image geodesics between points $(a^{\#}, b)$ and (a, b^*) respectively. A. Boundary points are taken to be $\phi_a = 5.1$, $t_a = -0.5$, $\phi_b = 0.6$, $t_b = 0.4$, parameter values are $\alpha = \pi/2$ and $\xi = 1.3$. B. Boundary points are taken to be $\phi_a = 5$, $t_a = -0.5$, $\phi_b = 1.6$, $t_b = 0.2$, parameter values are $\alpha = \pi/2$ and $\xi = 1.3$. C. Boundary points are taken to be $\phi_a = 4.4$, $t_a = -0.5$, $\phi_b = 1.6$, $t_b = 0.2$, parameter values are $\alpha = \pi/2$ and $\xi = 1.3$

case when the point a is on one of the faces of the wedge (for example on the bottom side) then the imaginary point a^* is on the upper side. The winding geodesic is a^*b.

There are three different combinations of image and basic geodesics contributing in the correlator on the boundary of the AdS_3 space deformed by the massive light particle:

- The basic geodesic contributes and the winding one does not.
- The basic geodesic does not contribute, and the winding one does.
- Both types of geodesics contribute in the correlator.

In Fig.12 we plot the different cases of geodesic configurations contributing to the propagator for certain values of α and ξ.

3.3.2 Heavy moving massive particle

If $\alpha > \pi$ the situation differs from the "light" case again. Here we get additional geodesic configurations contributing to the two-point function. The basic geodesic contribution is always present. For simplicity we consider here $\alpha = 3\pi/2$. Writing

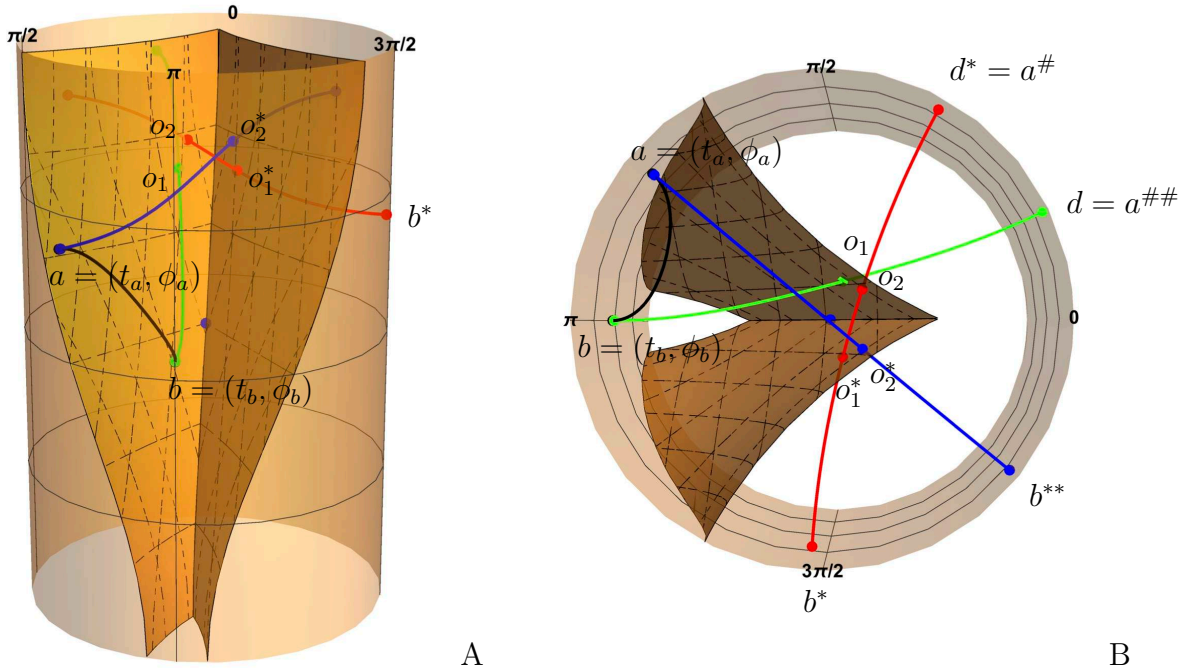

Figure 13. Double winding geodesic configuration connecting points a and b for certain boost ξ and mass parameter α. The parameter $\alpha = 5.4$. Black curve is basic geodesic and wound geodesic consists of three parts. The length of this geodesic is calculated as $l(a,b) = l(a,o_2^*) + l(o_2,o_1^*) + l(o_1,b)$.

down (3.16) explicitly we get the expression for the correlator

$$\begin{aligned}\mathfrak{G}_{\alpha,\xi}(\phi_a,t_a,\phi_b,t_b) &= G_{\Delta,AdS}(\phi_a,t_a,\phi_b,t_b)\,\Theta_0(\phi_a,t_a;\phi_b,t_b;\alpha,\xi) + \\ &+ G_{\Delta,ren,1}(\phi_a,t_a,\phi_b^*,t_b^*)\,\Theta_{cr}(t_a,\phi_a;t_b^*,\phi_b^*;\alpha,\xi) \\ &+ G_{\Delta,ren,1}(\phi_a,t_a,\phi_b^\#,t_b^\#)\,\Theta_{cr}(t_a,\phi_a;t_b^\#,\phi_b^\#;\alpha,\xi) \\ &+ G_{\Delta,ren,2}(\phi_a,t_a,\phi_b^{*2},t_b^{*2})\,\Theta_{cr}(\phi_a,t_a,\phi_b^{*2},t_b^{*2};\alpha,\xi) \\ &+ G_{\Delta,ren,2}(\phi_a,t_a,\phi_b^{\#2},t_b^{\#2})\,\Theta_{cr}(\phi_a,t_a,\phi_b^{\#2},t_b^{\#2};\alpha,\xi)\end{aligned}$$

The first term in (3.18) corresponds to the "basic geodesic", the second and third terms to the geodesic winding once, as in light particle case and the last two terms correspond to double winding geodesics. The last term contributes to the two-point function as can be seen in Fig.13.

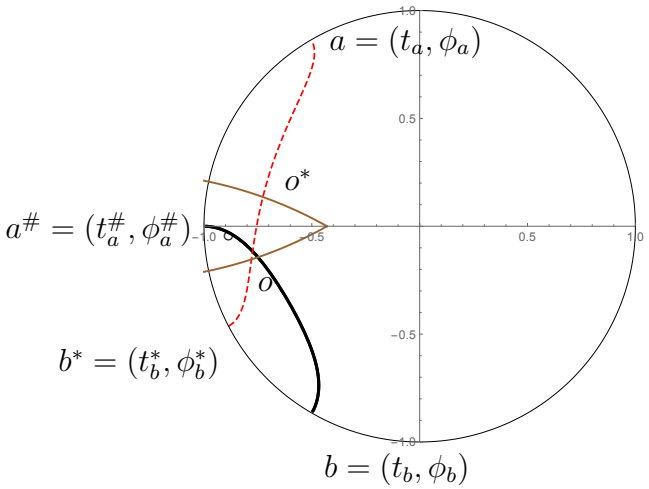

Figure 14. Geodesic connecting two boundary points following the points (b, o, o^*, a). Black curve is original geodesic and red dashed curve is geodesic between isometry points.

3.4 Renormalization

3.4.1 Spacelike geodesics

Now we consider the problem of finding the renormalized length of the image geodesic between two points on the boundary. Consider the geodesic between two near the boundary points (ϕ_a, t_a),(ϕ_b, t_b) that passes through the wedge. It can be represented as a geodesic consisting of two parts (see Fig.14) whose lengths are l_{a,o^*} and $l_{o,b}$. Here point o^* is the image of the point o under the isometry (2.12).

The isometry should respects the geodesic length between two points in the bulk i.e. $l_{o,b} = l_{o^*,b^*}$ therefore the length between points a and b must satisfy:

$$\mathcal{L}_{reg}(a, b) = \mathcal{L}_{reg}(a, b^*) = \mathcal{L}_{reg}(a^\#, b). \tag{3.18}$$

Here "reg" means the regularized length. The regularization means, as has been explained above, that we consider points a, b, $a^\#$ and b^* near the boundary. Expressions for renormalized lengths between points (a, b^*) and $(a^\#, b)$ are:

$$\begin{aligned} \mathcal{L}_{ren}(a, b^*) &= \ln 2[\cos(t_a - t_b^*) - \cos(\phi_a - \phi_b^*)], \\ \mathcal{L}_{ren}(a^\#, b) &= \ln 2[\cos(t_a^\# - t_b) - \cos(\phi_a^\# - \phi_b)]. \end{aligned} \tag{3.19}$$

It is obvious that these lengths are not equal. Let us do the calculations from the beginning taking into account the divergent part dependence on χ accurately. We define

$$\begin{aligned} \mathcal{L}_{ren}(a, b^*) &= \mathcal{L}_{reg}(a, b^*) - (\chi_a + \chi_{b^*}), \\ \mathcal{L}_{ren}(a^\#, b) &= \mathcal{L}_{reg}(a^\#, b) - (\chi_{a^\#} + \chi_b). \end{aligned} \tag{3.20}$$

The renormalized geodesic length between points a and b also is:

$$\mathcal{L}_{ren}(a, b) = \mathcal{L}_{reg}(a, b) - (\chi_a + \chi_b).$$

From (3.18) we can write:

$$\mathcal{L}_{ren}(a,b) = \mathcal{L}_{reg}(a^{\#},b) - (\chi_a + \chi_b) = \mathcal{L}_{reg}(a,b^{*}) - (\chi_a + \chi_b).$$

Substituting (3.19) in (3.20) we have:

$$\begin{aligned}\mathcal{L}_{ren}(a^{\#},b) &= \mathcal{L}_{ren}(a,b) - (\chi_{a^{\#}} + \chi_b) + \chi_a + \chi_b = \mathcal{L}_{ren}(a,b) + \chi_a - \chi_{a^{\#}}, \\ \mathcal{L}_{ren}(a,b^{*}) &= \mathcal{L}_{ren}(a,b) - (\chi_a + \chi_{b^{*}}) + \chi_a + \chi_b = \mathcal{L}_{ren}(a,b) + \chi_b - \chi_{b^{*}},\end{aligned} \tag{3.21}$$

and we obtain:

$$\mathcal{L}_{ren}(a^{\#},b) = \mathcal{L}_{ren}(a,b^{*}) + \chi_a - \chi_{a^{\#}} - \chi_b + \chi_{b^{*}}.$$

According to (2.16) for the large χ we have:

$$\begin{aligned}\chi_{b^{*}} &= \chi_b + \frac{1}{2}\ln C_{b^{*}},\ C_{b^{*}} = \left(\mathcal{B}_{\xi}(\alpha)\cos\phi_b + \sin t_b(1 + 2\sinh^2\xi\sin^2\frac{\alpha}{2})\right)^2 + \cos^2 t_b, \\ \chi_{a^{\#}} &= \chi_a + \frac{1}{2}\ln C_{a^{\#}},\ C_{a^{\#}} = \left(\mathcal{B}_{\xi}(-\alpha)\cos\phi_a + \sin t_a(1 + 2\sinh^2\xi\sin^2\frac{\alpha}{2})\right)^2 + \cos^2 t_a,\end{aligned}$$

where $\mathcal{B}_{\xi}(\alpha)$ is given by (2.14). Finally, using (3.21) we obtain the renormalized image geodesic length in the case of the removed regularization (for points a and b on the boundary):

$$\begin{aligned}\mathcal{L}_{ren}(a,b) &= \ln[2\left(\cos(t_a^{\#} - t_b) - \cos(\phi_a^{\#} - \phi_b)\right)C_{a^{\#}}^{1/2}] \\ &= \ln[2\left(\cos(t_a - t_b^{*}) - \cos(\phi_a - \phi_b^{*})\right)C_{b^{*}}^{1/2}].\end{aligned} \tag{3.22}$$

Let us consider the case when the geodesic passes few times through the faces of the wedge and then reach the boundary point forming multiple winding geodesics configuration. This is the case when massive particle deforming the AdS is heavy enough, i.e. $\alpha > \pi$. In Fig.13 we plot this situation. The geodesics of our interest consists of the pieces (b,o_1), (o_1^{*},o_2) and (o_2^{*},a). From the previous section we see, that each image of the point to be renormalized (let's assume point a) adds the factor $C_{a^{\#}}^{-1/2}$ for the $\#$ image and $C_{a^{*}}^{-1/2}$ for $*$. Thus for the two point function for the geodesic connecting a and b as it is show in Fig.13.B. we get the representation for factors Z_n and $\bar{Z}_n$ for multiple imaging geodesics:

$$\begin{aligned}Z_n(t_{a,n}^{\#},\phi_{a,n}^{\#};t_b,\phi_b) &= C_{a^{\#n}}^{-1/2} = C_{a^{\#(n-1)}}^{-1/2}C_{b^{*}}^{-1/2} = \ldots = C_{b^{*n}}^{-1/2} \\ \bar{Z}_n(t_{a,n}^{*},\phi_{a,n}^{*};t_b,\phi_b) &= C_{a^{*}}^{-1/2} = C_{a^{*(n-1)}}^{-1/2}C_{b^{\#}}^{-1/2} = \ldots = C_{b^{\#n}}^{-1/2}.\end{aligned} \tag{3.23}$$

3.4.2 Quasigeodesics

In this subsection we will find the renormalized length between timelike separated points (a and b). The length between points in the bulk can also be found, as in

the previous subsection, using (2.23). In accordance to Fig.15 the length consists of three parts and can be written as:

$$\mathcal{L}(a,b) = \mathcal{L}(a,h_1) + \mathcal{L}(h_2,o^*) + \mathcal{L}(o,b).$$

Taking in to account that the length is invariant under the isometry and also that points o and o^* are identical we get:

$$\mathcal{L}(o,b) = \mathcal{L}(o^*,b^*), \quad \mathcal{L}(a,b) = \mathcal{L}(a,h_1) + \mathcal{L}(h_2,b^*).$$

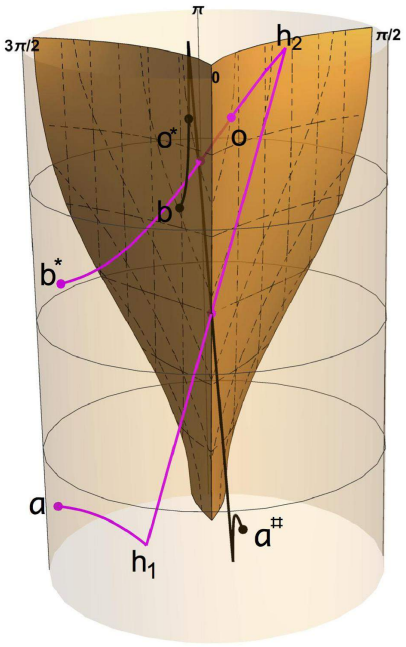

Figure 15. The plot of the quasigeodesic connecting a and b consists from the black curve between points $a^{\#}$ and b and the magenta curve between points a and b^*. Here we take parameter values: $\xi = 1$ and $\alpha = 1$.

According to (2.32) we can rewrite the lengths with divergent parts:

$$\mathcal{L}(a,h_1) = \mathcal{L}_{ren}(a,h_1) + \chi_a, \quad \mathcal{L}(b^*,h_2) = \mathcal{L}_{ren}(b^*,h_2) + \chi_{b^*}.$$

Taking into account expression (2.35) for renormalized length we can write:

$$\mathcal{L}(a,b) = \mathcal{L}(a,b^*) = \mathcal{L}(a,h_1) + \mathcal{L}(b^*,h_2) = \mathcal{L}_{ren}(a,b^*) + \chi_a + \chi_{b^*} - 2\ln 2. \quad (3.24)$$

On the other hand the formula for length between points a and b has a form:

$$\mathcal{L}(a,b) = \mathcal{L}_{ren}(a,b) + \chi_a + \chi_b - 2\ln 2. \quad (3.25)$$

From (3.24) and (3.25) we get the renormalized length for timelike separated points:

$$\mathcal{L}_{ren}(a,b) = \mathcal{L}_{ren}(a,b^*) - (\chi_b - \chi_{b^*}) = \mathcal{L}_{ren}(a,b^*) + \frac{1}{2}\ln C_{b^*}$$
$$= \ln[2|\cos(t_a - t_{b^*}) - \cos(\phi_a - \phi_{b^*})|C_{b^*}^{1/2}].$$

Also by the same way the formula for the renormalized geodesic length can be calculated using $a^{\#}$ and b points:

$$\mathcal{L}_{ren}(a,b) = \mathcal{L}_{ren}(a^{\#},b) - (\chi_a - \chi_{a^{\#}}) = \mathcal{L}_{ren}(a^{\#},b) + \frac{1}{2}\ln C_{a^{\#}}$$
$$= \ln[2|\cos(t_{a^{\#}} - t_b) - \cos(\phi_{a^{\#}} - \phi_b)|C_{a^{\#}}^{1/2}].$$

Therefore the formula for renormalization for quasigeodesics is (3.23) again.

4 Zone structure of correlators

4.1 Light particle

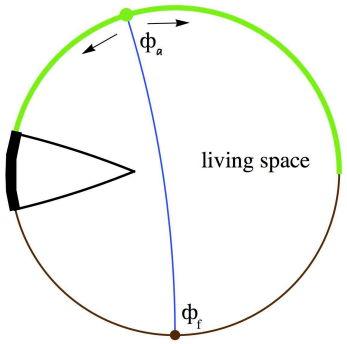

Figure 16. The schematic plot of locations of the moving massive light particle and two points that correlators depends on. The circle is the boundary of the constant time section of the AdS_3. The point ϕ_f is fixed on the brown part of the circle, ϕ_a varies in the green part of the circle. The removed arc is shown by the thick curve. The living space is indicated by the green and brown curves.

Let us consider the light moving particle and the case when points a and b are taken on the opposite sides of the boundary of AdS_3 (the opposite side means the opposite with respect to the massive particle worldline, see Fig.16 for the schematic plot).

As we have seen in the previous sections the deformation of the AdS_3 by moving particles produces changes of correlation functions of the boundary theory. To visualize these effect we depict the density plot of the inverse correlation function $\mathcal{G}_{\alpha,\xi,\phi_f,t_f}(\phi_a,t_a)$, as a function of coordinates of a point a and fixed coordinates (ϕ_f,t_f) and a variety of parameters α and ξ:

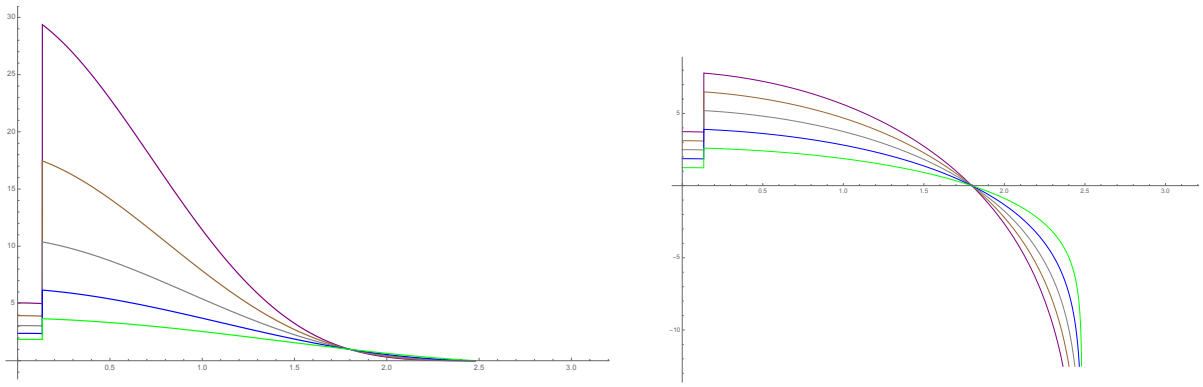

A B

Figure 17. A. Plots of $\mathcal{G}_{\alpha,\xi,\phi_f,t_f}(\phi_a,t_a)$ given by (4.1) as function of ϕ_a for fixed $t = 0.5$, $\phi_f = \frac{3\pi}{2}$ and $t_f = 0$, and parameters $\alpha = 0.3$, $\xi = 0.4$ for different values of Δ: $\Delta = 2.6, 2.2, 1.8, 1.4, 1$ (purple, brown, grey, blue and green lines, respectively). B. Plot of $\ln \mathcal{G}_{\alpha,\xi,\phi_f,t_f}(\phi_a,t_a)$ for the same parameters and $\Delta = 6, 5, 4, 3, 2$ (purple, brown, grey, blue and green lines, respectively). Thick vertical lines show the boundaries of the living space.

$$\mathcal{G}_{\alpha,\xi,\phi_f,t_f}(\phi_a,t_a) = G^{-1}_{\alpha,\xi}(\phi_a,t_a,\phi_f,t_f), \tag{4.1}$$
$$\phi_{max} < \phi_a < \pi, \qquad 2\pi - \phi_{max} < \pi < \phi_f < 2\pi, \qquad \alpha < \pi.$$

When a and f points are located on the opposite halves, the contribution coming from the image geodesic can appear and we can see effects related with the presence of the particle in the bulk (compare with discussion in [29]).

In Fig.17 we plot the function $\mathcal{G}_{\alpha,\xi,\phi_f,t_f}$ for fixed values of t_a, ϕ_f, t_f, α and ξ, and various Δ. In Fig.18 we present the density plots of the function $\mathcal{G}_{\alpha,\xi,\phi_f,t_f}$ for certain values of ϕ_f, t_f, α, ξ and $\Delta = 1$. The red curves correspond to the boundary of the removed zone, black curves indicate locations of discontinuities separating different zones.

In each plot in Fig.18 there is a zone, where the basic geodesic contribute only, i.e. the correlation function remains unchanged, and there is a zone (next to the $\phi = 0$) where the winding geodesic contributes. These regions are separated by discontinuities. The white zone appears when the points on the boundary are timelike separated.

4.2 Heavy particle

For the heavy particle we study the similar correlator as for the light particle in the previous section, but in the different region

$$\mathcal{G}_{\alpha,\xi,\phi_f,t_f}(\phi_a,t_a) = G^{-1}_{\alpha,\xi}(\phi_a,t_a,\phi_f,t_f) \tag{4.2}$$
$$0 < \phi_a < 2\pi, \quad \frac{\pi}{2} < \phi_f < \frac{3\pi}{2}, \quad \alpha = \frac{3\pi}{2} > \pi.$$

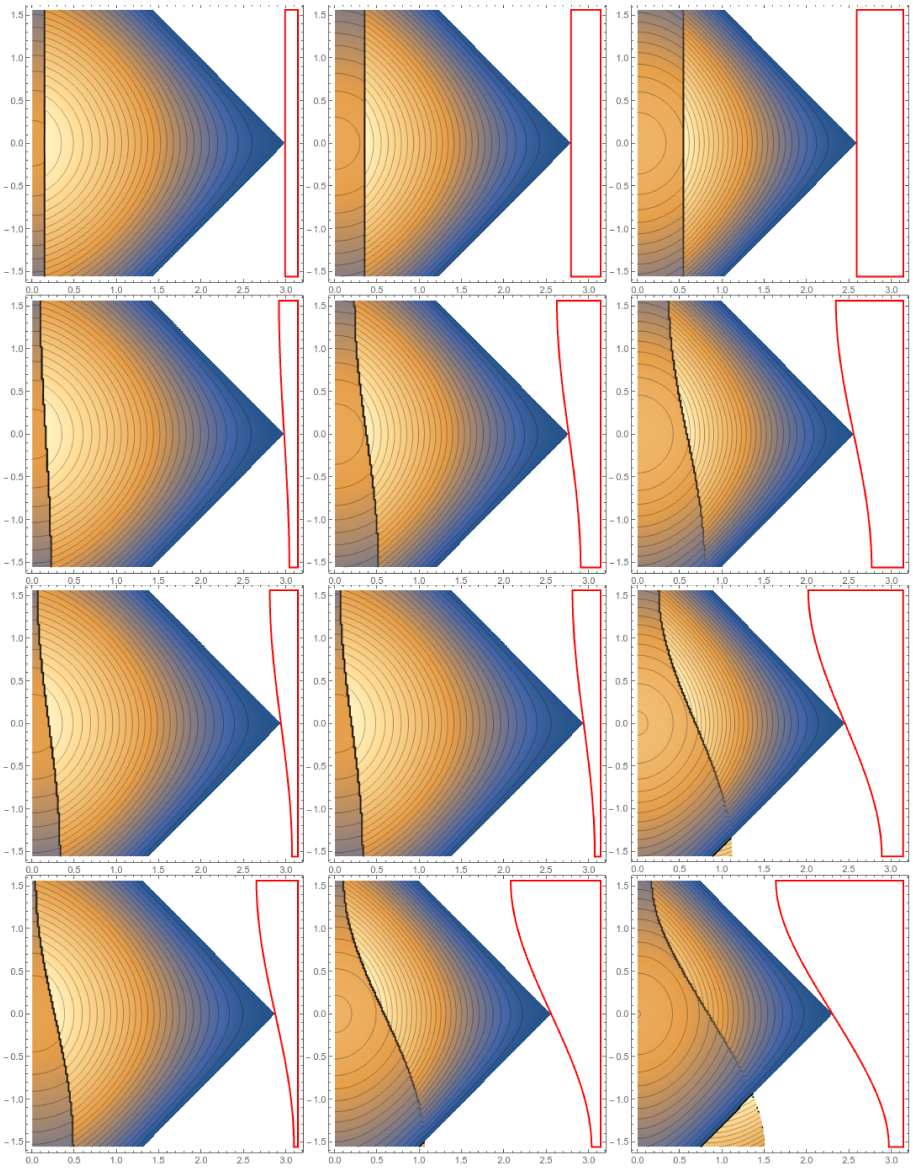

Figure 18. The density plots of function $\mathcal{G}_{\alpha,\xi,\phi_f,t_f}(\phi_a, t_a)$ given by (4.1) for different values of α and ξ. The parameter α increases from the left to right, corresponding to $\alpha = 0.3, 0.7, 1.1$. The parameter ξ increases from top to down, corresponding to $\xi = 0, 0.4, 0.8, 1.2$. On each plot ϕ_a corresponds to x-axis and t_a to y-axis, $\phi_f = 3\pi/2$ and $t_f = 0$. The red thick curves correspond to the boundaries of the living spaces.

The zone structure of the 2-point correlator on the boundary of AdS_3 with a heavy moving particle is presented in Fig.20 and Fig.21. In these plots we see, that

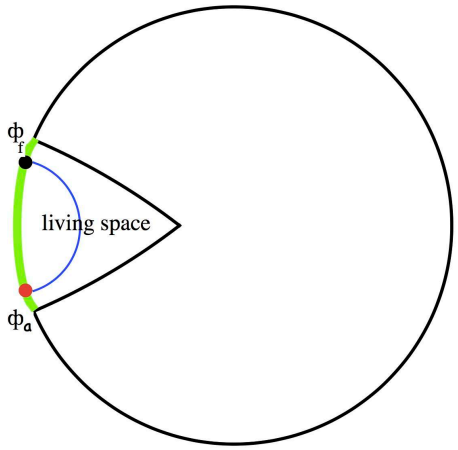

Figure 19. The schematic plot of locations of the moving massive heavy particle and two points of the correlator. The circle is the boundary of the AdS_3 at a constant time section, the point ϕ_f is fixed in the living space, the green part of the AdS_3 boundary. The point ϕ_a belongs to the living area too.

there are several different zones. These zones are typical for heavy particle deformations, and the origin of these zones can be explained first on the static particle, see Fig.22 and Fig.23.

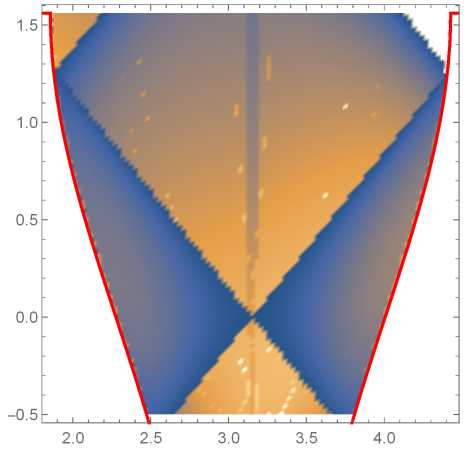

Figure 20. The density plot of the function $\mathcal{G}_{\alpha,\xi,\phi_f,t_f}(\phi_a, t_a)$ given by (4.2). Here $\phi_f = \pi$ and $t_f = 0$ and $\alpha = \frac{3\pi}{2}$, and $\xi = 0.6$, ϕ_a corresponds to x-axis and t_a to y-axis, the red thick curves show the boundaries of the removed areas.

Let us take the point a in the darkest zone, see Fig.23. The points a and b are spacelike separated points. The point a can be connected by geodesics not only with the point b, with coordinates $\phi_b = \phi_f = \pi$, $t_b = t_f = 0$, but also with the image points b^*, b^{**} and $b^{\#}$, and there are several contributions to the propagator. For the case presented in Fig.23, there are contributions from 4 terms.

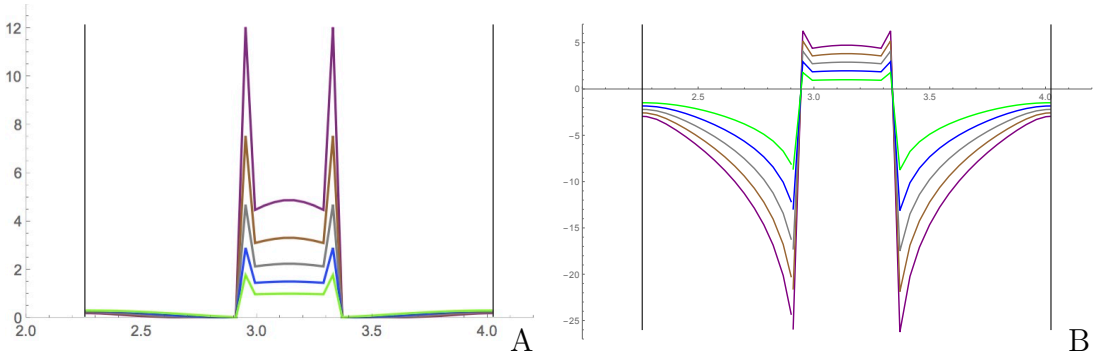

Figure 21. A. Plots of $\mathcal{G}_{\alpha,\xi,\phi_f,t_f}(\phi_a,t_a)$ given by (4.2) as function of ϕ_a for fixed $t_a = 0.2$, $\phi_f = \pi$ and $t_f = 0$, and parameters $\alpha = 3\pi/2$, $\xi = 0.4$ for different values of Δ: $\Delta = 2.6, 2.2, 1.8, 1.4, 1$ (purple, brown, grey, blue and green lines, respectively). B. Plot of $\ln \mathcal{G}_{\alpha,\xi,\phi_f,t_f}(\phi_a,t_a)$ for the same parameters and $\Delta = 6, 5, 4, 3, 2$ (purple, brown, grey, blue and green lines, respectively). Thick vertical lines show the boundaries of the living space.

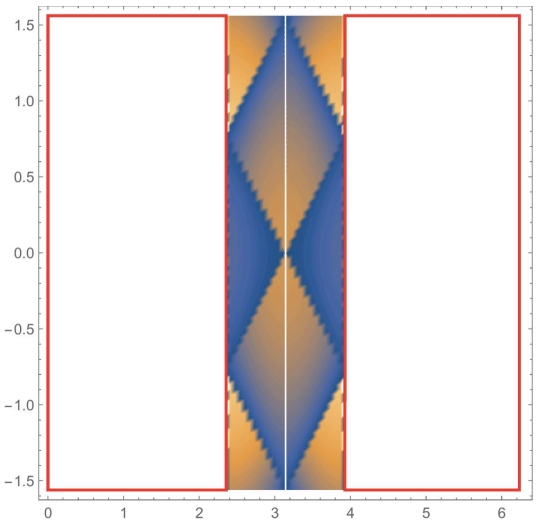

Figure 22. The density plot of the function $\mathcal{G}(a,b)$ on the living space in case of the static heavy particle. In the plot $\alpha = 3\pi/2$, $\phi_f = \pi$ and $t_f = 0$. Here ϕ_a corresponds to x-axis and t_a to y-axis. Note, that the scales on x-axis and y-axis are different. The red thick rectangle show the removed parts of the AdS boundary.

Let us consider the moving heavy particle located at the initial time as shown in Fig.19. Now the living space may be located only in the interval $(\pi/2, 3\pi/2)$. In Fig.24 we plot contributions for different geodesics configurations. In this figure we see that the basic spacelike geodesics contribution is bounded by lightcone, the single winding geodesic contributes almost everywhere, contributions from different double winding geodesic configurations form zones near the boundary, but the total double winding geodesics contribution covers all the living space. In Fig.20 we show the sum of all contributions presented separately in Fig.24. In the Fig.21 the two dimensional

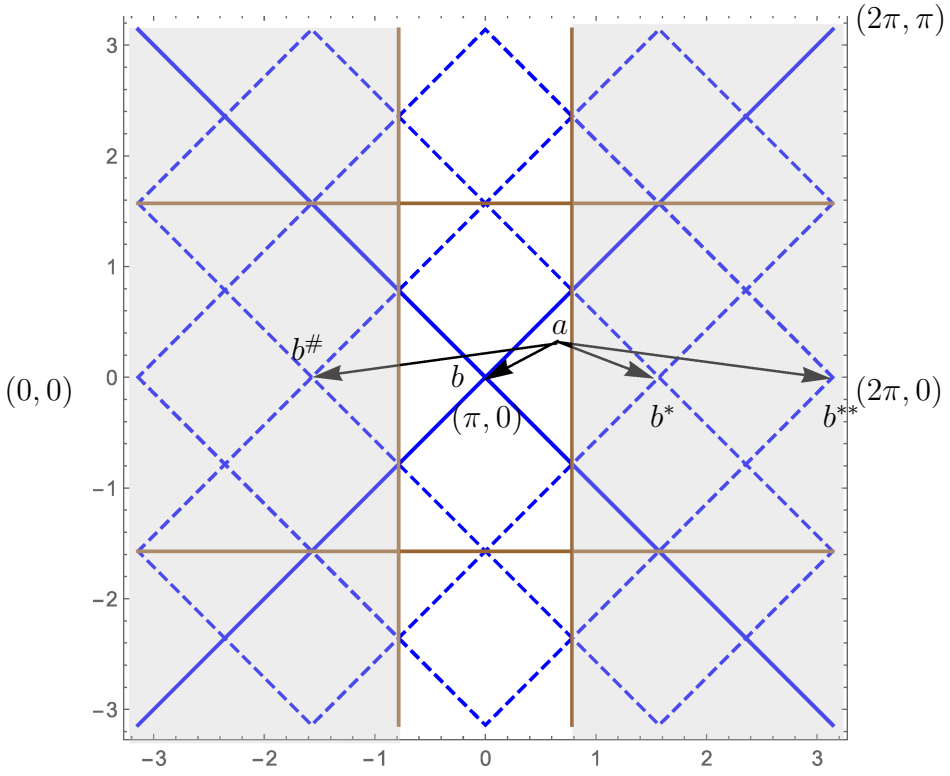

Figure 23. The schematic plot of different zones of the 2-point correlation function. Here the scales along x-axis and y-axis are the same.

plot of the inverse correlation function for the several values of Δ and for the fixed parameters α and ξ is presented for the case of massive particle. Remind that we do not consider the geodesics between timelike separated points.

From the plot in Fig.20 we see that for the heavy particle there is no any "shadow" like in the light particle case.

5 Conclusion

In this paper we have investigated the correlation functions of conformal operators in the theory dual to the AdS_3 deformed by moving massive particles. Our calculations are based on the geodesic approximation. This approximation works well for operators with large conformal dimension Δ. However, we have considered how this approximation works starting from $\Delta = 1$. We find, that the 2-point correlation function gets additional contributions due to the nontrivial geodesic structure of the deformed spacetime. The presence of these additional geodesics does not depend on the conformal dimension. The additional geodesics are found via the renormalized image method. In the work we did not take into account the contribution of geodesics between timelike separated points.

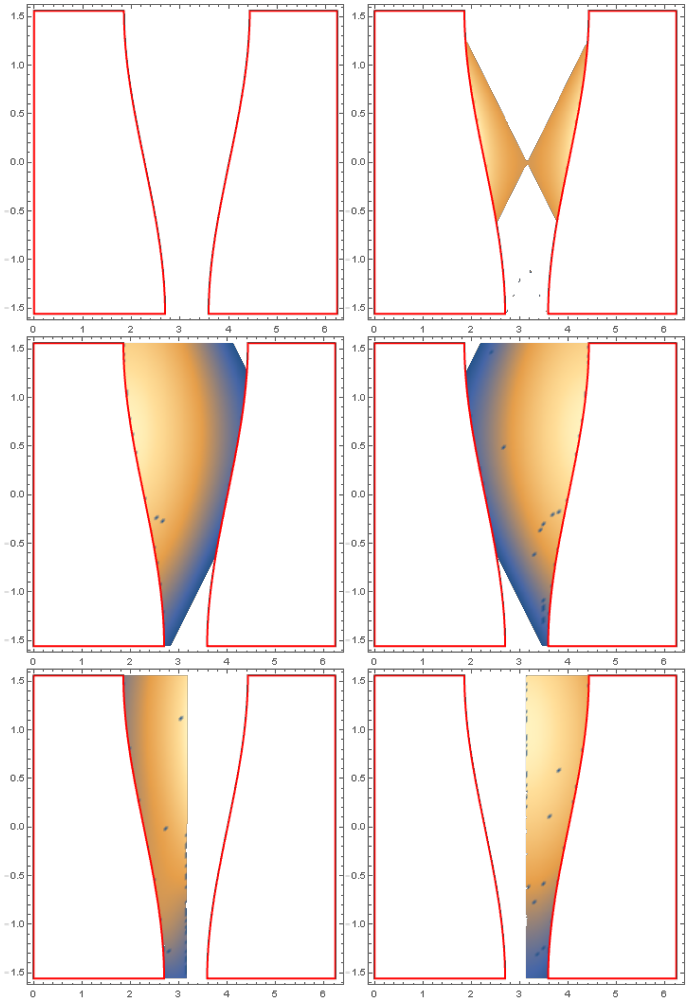

Figure 24. The density plots of separate contributions to the function (4.2). For each plot $\phi_f = \pi$, $t_f = 0$, $\alpha = \frac{3\pi}{2}$ and $\xi = 0.6$. On each plot ϕ_a corresponds to x-axis and t_a to y-axis, the red thick curves correspond to the boundaries of the removed areas. The bottom left plot shows the boundary of the removed area, the bottom right shows the contribution from the basic geodesic, the left and right plots in the second row show contributions of double winding geodesics coming from different terms in (4.2), the third row shows the single winding geodesic.

We get two different pictures of behaviour of the 2-point correlators on the boundary of AdS_3 deformed by moving/static particles. The first case, is when the particle deforming the AdS_3 is light. In this case additional contributions mentioned above give us to the following picture: we have two different zones separated by discontinuity. One of the zones corresponds to the original correlator of the conformal field on the cylinder. Another zone corresponds to the deformed theory, i.e. constant level lines of the inverse correlator are slightly deformed. The second case is the case of the heavy particle. In this case 2-point correlator differs qualitatively: it is

deformed in a whole space and there are many different contributions from different multiple winding geodesics. The number of winding depends on the ratio $2\pi/\bar{\alpha}$, where $\bar{\alpha}$ is the angle of the living space.

It is interesting to compare the results presented in the paper with correlators obtained using the scalar field in the bulk via the GKPW prescription [2, 3]. This is a subject of paper [44]. The image method for timelike separated points and a continuation of correlators to the entire boundary have been considered in the paper [45]

Acknowlegement

We would like to thank Andrey Bagrov, Dmitry Bykov, Xian Otero Camanho, Mikhail Khramtsov, Andrey Mikhailov, Giuseppe Policastro and Igor Volovich for useful discussions. This work is supported by the RFBR grant 14-01-00707 and grant MK-2510.2014.1 (D.S.A.) of the President of Russia Grant Council. I.Ya. A. thanks the Galileo Galilei Institute for Theoretical Physics for the hospitality and the INFN for partial support during the preparation of this work.

References

[1] J. M. Maldacena, "The Large N limit of superconformal field theories and supergravity," Adv. Theor. Math. Phys. **2**, 231-252 (1998), [hep-th/9711200].

[2] S. S. Gubser, I. R. Klebanov, A. M. Polyakov, "Gauge theory correlators from noncritical string theory," Phys. Lett. **B428**, 105-114 (1998), [hep-th/9802109].

[3] E. Witten, "Anti-de Sitter space and holography," Adv. Theor. Math. Phys. **2**, 253-291 (1998), [hep-th/9802150].

[4] I. Ya. Aref'eva, "Holographic approach to quark-gluon plasma in heavy ion collisions," Phys. Usp. **57**, 527 (2014).

[5] O. DeWolfe, S. S. Gubser, C. Rosen and D. Teaney, "Heavy ions and string theory," Prog. Part. Nucl. Phys. **75**, 86 (2014) [arXiv:1304.7794 [hep-th]].

[6] J. Casalderrey-Solana, H. Liu, D. Mateos, K. Rajagopal, U. A. Wiedemann, "Gauge/String Duality, Hot QCD and Heavy Ion Collisions," [arXiv:1101.0618 [hep-th]].

[7] C. P. Herzog, P. Kovtun, S. Sachdev and D. T. Son, "Quantum critical transport, duality, and M-theory," Phys. Rev. D **75**, 085020 (2007) [hep-th/0701036].

[8] S. A. Hartnoll, C. P. Herzog and G. T. Horowitz, "Building a Holographic Superconductor," Phys. Rev. Lett. **101**, 031601 (2008) [arXiv:0803.3295 [hep-th]].

[9] S. A. Hartnoll, C. P. Herzog and G. T. Horowitz, "Holographic Superconductors," JHEP **0812**, 015 (2008) [arXiv:0810.1563 [hep-th]].

[10] V. Balasubramanian *et al.*, "Holographic Thermalization," Phys. Rev. D **84**, 026010 (2011) [arXiv:1103.2683 [hep-th]].

[11] V. Balasubramanian *et al.*, "Thermalization of the spectral function in strongly coupled two dimensional conformal field theories," JHEP **1304**, 069 (2013) [arXiv:1212.6066 [hep-th]].

[12] J. Aparicio and E. Lopez, "Evolution of Two-Point Functions from Holography," JHEP **1112**, 082 (2011), [arXiv:1109.3571 [hep-th]].

[13] V. Keranen, E. Keski-Vakkuri and L. Thorlacius, "Thermalization and entanglement following a non-relativistic holographic quench," Phys. Rev. D **85**, 026005 (2012), [arXiv:1110.5035 [hep-th]].

[14] I. Y. Aref'eva, "QGP time formation in holographic shock waves model of heavy ion collisions," TMF, 182 (2015), 3, arXiv:1503.02185 [hep-th].

[15] S. Ryu and T. Takayanagi, "Holographic derivation of entanglement entropy from AdS/CFT," Phys. Rev. Lett. **96**, 181602 (2006) [hep-th/0603001].

[16] S. Ryu and T. Takayanagi, "Aspects of Holographic Entanglement Entropy," JHEP **0608**, 045 (2006) [hep-th/0605073].

[17] T. Nishioka, S. Ryu and T. Takayanagi, "Holographic Entanglement Entropy: An Overview," J. Phys. A **42**, 504008 (2009) [arXiv:0905.0932 [hep-th]].

[18] P. Calabrese and J. L. Cardy, "Entanglement and correlation functions following a local quench: a conformal field theory approach", J. Stat. Mech. 10 (2007) P10004, arXiv:0708.3750.

[19] M. Nozaki, T. Numasawa and T. Takayanagi, "Holographic Local Quenches and Entanglement Density," JHEP **1305**, 080 (2013) [arXiv:1302.5703 [hep-th]].

[20] S. Deser, R. Jackiw, and G. 't Hooft, "Three dimensional Einstein gravity: dynamics of flat space", *Ann. Phys.* **152** (1984) 220

[21] G. 't Hooft, "Quantization of point particles in (2+1)-dimensional gravity", *Class. Quantum Grav.* **13** (1996) 1023.

[22] S. Deser and R. Jackiw, "Classical and Quantum Scattering on a Cone," Commun. Math. Phys. **118**, 495 (1988).

[23] J. S. Dowker, "Quantum Field Theory on a Cone", J. Phys. A 10, 115 (1977)

[24] M. O. Katanaev and I.V. Volovich, Theory of defects in solids and three-dimensional gravity, Ann. of Phys., NY, 216 (1992) 1

[25] Kibble T. W. B. Topology of cosmic domains and string. J. Phys. A 9 (1976) 1387

[26] I. Kirsch, "Generalizations of the AdS / CFT correspondence," Fortsch. Phys. **52**, 727 (2004), hep-th/0406274.

[27] C. A. B. Bayona, C. N. Ferreira and V. J. V. Otoya, "A Conical deficit in the AdS(4)/CFT(3) correspondence," Class. Quant. Grav. **28**, 015011 (2011) [arXiv:1003.5396 [hep-th]].

[28] I. Ya. Aref'eva, Colliding hadrons as cosmic membranes and possible signatures of lost momentum, Springer Proceedings in Physics, 137 (2011) 21; arXiv: 1007.4777

[29] V. Balasubramanian and S. F. Ross, "Holographic particle detection," Phys. Rev. D **61**, 044007 (2000) [hep-th/9906226].

[30] I.Ya. Aref'eva and A. A. Bagrov, Holographic dual of a conical defect, Theoret. and Math. Phys., 182 (2015), 22

[31] V. Balasubramanian, A. Naqvi and J. Simon, "A Multiboundary AdS orbifold and DLCQ holography: A Universal holographic description of extremal black hole horizons," JHEP **0408** (2004) 023 [hep-th/0311237].

[32] V. Balasubramanian, B. D. Chowdhury, B. Czech and J. de Boer, "Entwinement and the emergence of spacetime," JHEP **1501**, 048 (2015)

[33] I. Arefeva, A. Bagrov, P. Saterskog and K. Schalm, "Holographic dual of a time machine," arXiv:1508.04440 [hep-th].

[34] M. Araujo, D. Arean, J. Erdmenger and J. M. Lizana, "Holographic charge localization at brane intersections," JHEP **1508**, 146 (2015) [arXiv:1505.05883 [hep-th]].

[35] H. J. Matschull, "Black hole creation in (2+1)-dimensions," Class. Quant. Grav. **16**, 1069 (1999); gr-qc/9809087.

[36] H. J. Matschull and M. Welling, "Quantum mechanics of a point particle in (2+1)-dimensional gravity," Class. Quant. Grav. **15**, 2981 (1998); gr-qc/9708054.

[37] M. Ciafaloni, "N body solutions of 2+1 gravity," Nucl. Phys. Proc. Suppl. **57**, 323 (1997).

[38] K. Osterwalder and R. Schrader, "Axioms For Euclidean Green's Functions," Commun. Math. Phys. **31**, 83 (1973). K. Osterwalder and R. Schrader, "Axioms for Euclidean Green's Functions. 2.," Commun. Math. Phys. **42**, 281 (1975).

[39] M. Luscher and G. Mack, "Global Conformal Invariance in Quantum Field Theory," Commun. Math. Phys. **41**, 203 (1975).

[40] R. Haag, Local quantum physics: Fields, particles, algebras, Berlin, Germany: Springer (1992) 356 p.

[41] I.M. Gelfand and G.E. Shilov, Generalized Functions, Vol. 1, Academic Press, New York (1964).

[42] K. Skenderis and B. C. van Rees, "Real-time gauge/gravity duality: Prescription, Renormalization and Examples," JHEP **0905**, 085 (2009) [arXiv:0812.2909 [hep-th]].

[43] D. S. Ageev and I. Ya. Aref'eva, "Holographic dual to conical defects: II Colliding Ultrarelativistic Particles," [arXiv:1512.03363 [hep-th]]

[44] I. Ya. Aref'eva and M. A. Khramtsov, "AdS/CFT prescription for angle-deficit space and winding geodesics," JHEP **1604**, 121 (2016) [arXiv:1601.02008 [hep-th]]

[45] I. Ya. Arefeva, M. A. Khramtsov and M. D. Tikhanovskaya, "Holographic Dual to Conical Defects III: Improved Image Method," [arXiv:1604.08905 [hep-th]]